UAB
Universitat Autònoma de Barcelona

Dipòsit digital de documents de la UAB

This is the **accepted version** of the journal article:

Blázquez-Pallí, Natàlia (LITOCLEAN, S.L.); Torrentó, Clara; Marco Urrea, Ernest; [et al.]. «Pilot tests for the optimization of the bioremediation strategy of a multi-layered aquifer at a multi-focus site impacted with chlorinated ethenes». Science of the Total Environment, Vol. 935 (July 2024), art. 173093. 68 pàg. DOI 10.1016/j.scitotenv.2024.173093

This version is available at https://ddd.uab.cat/record/292653

under the terms of the BY-NC-ND license

Manuscript (double-spaced and continuously LINE and PAGE numbered)-for final publication

Click here to view linked References

1 **Title**

2 Pilot tests for the optimization of the bioremediation strategy of a multi-
3 layered aquifer at a multi-focus site impacted with chlorinated ethenes

4 Authors:

5 Natàlia Blázquez-Pallí[a,*], Clara Torrentó[b,c], Ernest Marco-Urrea[d], David
6 Garriga[a], Marta González[a], Marçal Bosch[a]

7

8 [a]LITOCLEAN, S.L., Environmental site assessment and remediation, c/ Numància 36, 08029 Barcelona,
9 Spain.

10 [b]Grup MAiMA, SGR Mineralogia Aplicada, Geoquímica i Hidrogeologia (MAGH), Departament de
11 Mineralogia, Petrologia i Geologia Aplicada, Facultat de Ciències de la Terra, Institut de Recerca de
12 l'Aigua (IdRA), Universitat de Barcelona (UB), Martí Franquès s/n, 08028 Barcelona, Spain.

13 [c]Serra Húnter Fellowship, Generalitat de Catalunya, Spain.

14 [d]Departament d'Enginyeria Química, Biològica i Ambiental, Universitat Autònoma de Barcelona (UAB), c/
15 de les Sitges s/n, 08193 Cerdanyola del Vallès, Spain.

16 ** Corresponding author: Natàlia Blázquez-Pallí, e-mail: nblazquez@litoclean.es, full postal address: c/
17 Numància 36, 08029 Barcelona, Spain.*

18

19 **Abstract – 300 words**

20 A multi-layered aquifer in an industrial area in the north of the Iberian Peninsula is severely
21 contaminated with the chlorinated ethenes (CEs) tetrachloroethylene, trichloroethylene, *cis*-1,2-
22 dichloroethylene, and vinyl chloride. Both shallow and deep aquifers are polluted, with two
23 differentiated north and south CEs plumes. Hydrogeochemical and isotopic data ($\delta^{13}C$ of CEs)
24 evidenced natural attenuation of CEs. To select the optimal remediation strategy to clean-up the
25 contamination plumes, laboratory treatability studies were performed, which confirmed the
26 intrinsic biodegradation potential of the north and south shallow aquifers to fully dechlorinate
27 CEs to ethene after injection of lactate, but also the combination of lactate and sulfidized mZVI

as an alternative treatment for the north deep aquifer. In the lactate-amended microcosms, full dechlorination of CEs was accompanied by an increase in 16S rRNA gene copies of *Dehalococcoides* and *Dehalogenimonas*, and the *tceA*, *vcrA* and *bvcA* reductive dehalogenases. Three *in situ* pilot tests were implemented, which consisted in injections of lactate in the north and south shallow aquifers, and injections of lactate and sulfidized mZVI in the north deep aquifer. The hydrogeochemical, isotopic and molecular analyses used to monitor the pilot tests evidenced that results obtained mimicked the laboratory observations, albeit at different dechlorination rates. It is likely that the efficiency of the injections was affected by the amendment distribution. In addition, monitoring of the pilot tests in the shallow aquifers showed the release of CEs due to back diffusion from secondary sources, which limited the use of isotopic data for assessing treatment efficiency. In the pilot test that combined the injection of lactate and sulfidized mZVI, both biotic and abiotic pathways contributed to the production of ethene. This study demonstrates the usefulness of integrating different chemical, isotopic and biomolecular approaches for a more robust selection and implementation of optimal remediation strategies in CEs polluted sites.

Keywords: chlorinated aliphatic hydrocarbons, groundwater contamination, biostimulation, in situ chemical reduction, Dehalococcoides, Dehalogenimonas

1. Introduction

Southern Europe is experiencing a persistent drought, with severe and critical conditions in most of the Mediterranean region (European Commission, 2022). In this area, groundwater is of critical importance because it is the primary source of water supply for many communities and ecosystems (European Commission, 2007), and efforts are made to remediate contaminated groundwater to protect this valuable resource. Halogenated organic compounds are commonly found in different environmental compartments (soils, groundwater, surface water) because of current spills or legacy contamination derived from their use in industry and agriculture (Loganathan and Lam, 2011). The widespread contamination of soils and groundwaters by anthropogenic halogenated compounds has been previously described (Moran, 2006; Moran et

al., 2007; Panagos et al., 2013; Zogorski et al., 2006). One of the most ubiquitous families of anthropogenic halogenated compounds detected in groundwaters are chlorinated ethenes (CEs, Table 1) (Bouwer, 1994; McCarty and Semprini, 1994; Vogel, 1994), from which perchloroethylene (PCE) and trichloroethylene (TCE) are the ones more frequently detected at significant concentrations and/or in the form of dense non-aqueous phase liquid (DNAPL) (Bradley, 2000). Due to the incomplete dechlorination of PCE and TCE by natural biotic or abiotic attenuation processes in the subsoil, the lesser CEs cis-1,2-dichloroethylene (*cis*-DCE) and vinyl chloride (VC) can accumulate in soil and groundwater, albeit usually at lower concentrations (Bradley, 2000; Leeson et al., 2004; Mattes et al., 2010). All these substances are considered toxic and are listed as priority substances by several international agencies and institutions (ATSDR, 2022; European Commission, 2008; US EPA, 2014) and, therefore, maximum concentration levels in soils and groundwater have been set by environmental agencies worldwide.

PCE is biologically recalcitrant under oxic conditions, but can undergo biotic and abiotic transformation reactions under anoxic conditions (Bradley, 2000; Mattes et al., 2010). Biotically, the degradation pathway occurs via reductive dechlorination through hydrogenolysis, which is performed by a variety of organohalide respiring bacteria (OHRB), and consists on the sequential cleavage of the C–Cl bonds in the PCE molecule and the simultaneous addition of a hydrogen atom, resulting in the production of lesser chlorinated compounds (Adrian and Löffler, 2016). However, the ability to fully dechlorinate CEs to the non-toxic alkane gas ethene (ETH) is known to be limited to only two OHRB genera: *Dehalococcoides* sp. (*Dhc*) (Löffler et al., 2013b; Zinder, 2016) and, more recently, *Dehalogenimonas etheniformans* (Chen et al., 2022; Cui et al., 2023; Yang et al., 2017b). In *in situ* bioremediation treatments for CEs-contaminated sites, which use the metabolism of OHRB to remediate contamination, the genes that encode the reductive dehalogenase enzymes driving organohalide respiration can be used as biomarkers to assess the occurrence and performance of these transformation reactions. For instance, the presence and/or quantification of the reductive dehalogenases *PceA*, *TceA*, and *BvcA* and/or *VcrA* can be used to assess the potential and/or confirm the occurrence of the partial reactions of PCE to TCE, TCE to VC, and VC to ETH, respectively (Cupples, 2008; Hug et al., 2013; Hug and Edwards, 2013; Krajmalnik-Brown et al., 2004; Muller et al., 2004; Yan et al., 2021). Other

bacterial genera have been described to partially dechlorinate some CEs (Atashgahi et al., 2016; Holliger et al., 2004; Löffler et al., 2013a, 2004; Smidt and de Vos, 2004), but these incomplete reactions can lead to the accumulation of toxic intermediates in the subsoil, a phenomenon that has been historically referred to as "*cis*-DCE or VC stall" (Bradley, 2000; Stroo and Ward, 2010), depending on the intermediate generated. These stalls can also be observed when the hydrogeochemical conditions of the aquifer are not appropriate (e.g., insufficiency of electron donor/carbon source that leads to mild anaerobic conditions). In these instances, amendments such as organic fermentable substrates can be injected into the subsurface to enhance reductive dechlorination (Adrian and Löffler, 2016; Leeson et al., 2004).

If OHRB or the corresponding functional genes required to complete the degradation of CEs are not present, the abiotic alternative (also referred to as *in situ* chemical reduction, ISCR) can also be efficient under the same hydrogeochemical conditions (i.e., anoxia, sulphate-reduction and methanogenesis). In the abiotic process, which requires the presence of reduced minerals, PCE is sequentially transformed to ETH and ethane through the hydrogenolysis and/or β-dichloroelimination pathways, which circumvents VC formation by transforming *cis*-DCE to acetylene (Arnold and Roberts, 2000; Audí-Miró et al., 2013; Elsner et al., 2008). However, the abiotic degradation mechanisms of CEs are complex and can result in different end-products depending on the reaction conditions (Elsner et al., 2008; Herrero et al., 2019; VanStone et al., 2004; Vogel et al., 1987). If this process is not occurring naturally, it can also be enhanced with the addition of inorganic amendments (usually iron-based) such as micro- or nanoscale zero-valent iron (mZVI, nZVI), sulfidized mZVI or nZVI, or soluble Fe(II), among others (Brown, 2010; Fu et al., 2014; Galdames et al., 2020; Guo et al., 2023). In field applications, the combined addition of ZVI with an organic substrate is recommended (Herrero et al., 2019; Wang et al., 2016), but field studies of this technology are scarce (Kocur et al., 2016; Sheu et al., 2016; Wu et al., 2020; Yang et al., 2018).

In order to adequately assess the occurrence and extent of biotic and abiotic CEs degradation reactions, it is encouraged to provide several lines of evidence of such transformations (Bombach et al., 2010; Nijenhuis and Kuntze, 2016). Besides the analysis of the physicochemical conditions of groundwater, contaminant concentrations, and the already mentioned biomarkers, compound-specific stable isotope analysis (CSIA) is also a useful tool to

provide direct evidence of degradation of many contaminants, including CEs (Kuntze et al., 2019; Nijenhuis and Richnow, 2016). CSIA measures the ratio of stable isotopes (e.g. $^{13}C/^{12}C$) of a contaminant relative to an international standard, resulting in the isotopic composition (δ) of such molecule (Aelion et al., 2009). This technique relies on the fact that molecules containing lighter isotopes are transformed at a higher rate than molecules containing heavier isotopes and, thus, significant shifts in the isotopic composition are an irrefutable evidence of degradation reactions (Elsner, 2010). Furthermore, it is also possible to estimate the contaminant transformation extent in the field (%D), as long as the isotope fractionation (ε) for a specific compound and degradation pathway is available (Aelion et al., 2009). Thus, CSIA is a useful tool for practitioners to assess the occurrence and effectiveness of biological and chemical *in situ* remediation treatments.

Even though the aforementioned standalone techniques have been applied in the remediation sector for several decades, their combination in an integrative approach is still not mainstream because some of them are still not "market-ready", are relatively expensive, and require of transdisciplinary expertise. For instance, the combined use of diverse monitoring methods has been demonstrated successful for the characterization of contaminated sites and/or the assessment of the potential of remediation strategies in the laboratory (Abe et al., 2009; Badin et al., 2016; Blázquez-Pallí et al., 2019a, 2019c; Buchner et al., 2015; Imfeld et al., 2008; Lee et al., 2016; Matteucci et al., 2015; McKelvie et al., 2007; Nijenhuis et al., 2007; Tarnawski et al., 2016; Trueba-Santiso et al., 2022; Yu et al., 2018). However, few integrative studies are available using these lines of evidence in the field for the monitoring of *in situ* bioremediation implementations (Blázquez-Pallí et al., 2019b; Herrero et al., 2019; Madison et al., 2023; Ottosen et al., 2021; Yang et al., 2018).

For this reason, this study aims to implement and validate this multi-method approach in a complex real scenario to delineate the optimal bioremediation strategy to be applied full-scale. Specifically, the objectives of this study were: 1) to assess whether natural attenuation was occurring at a multi-focus and multi-layered aquifer CEs-contaminated site, 2) to evaluate the intrinsic biodegradation potential and the feasibility of different *in situ* remediation strategies, including bioremediation alone, and in combination with ISCR (hereinafter, B-ISCR), and 3) to implement three different *in situ* pilot tests with the selected bioremediation strategy based on

147 the preceding points. Throughout this study, the integrative monitoring methodology used
148 included: i) hydrogeochemical characterization; ii) treatability microcosm experiments; iii)
149 molecular techniques (qPCR and metabarcoding); and iv) CSIA ($\delta^{13}C$ of CEs).

150 **2. Material and methods**

151 *2.1. Study site*

152 The studied site is a historical multi-industrial area located in the north of the Iberian
153 Peninsula, where the shallow aquifer is severely contaminated with the CEs PCE, TCE, *cis*-
154 DCE and VC. Due to its location and characteristics, the area is of strategic importance: it is
155 really close to the coast, belongs to a protected area, and the deep aquifer, also impacted
156 with CEs, is exploited for water supply. Throughout the studied area, two different
157 hydrological units can be found: the upper one, constituted by anthropic fill, and silts and
158 clays, corresponds to the shallow aquifer; whereas the lower one, constituted by a layer of
159 alluvial base gravels and Jurassic materials, corresponds to the deep aquifer. This
160 permeable lithologic unit of gravels constitutes the main CEs migration pathway, vertically
161 and horizontally, the latter being greatly affected by the pumping regime of the nearby deep
162 aquifer exploitation wells (Supplementary Information, SI, Fig. S1). Two differentiated north
163 and south CEs plumes have been identified. To date, in both the north and south areas,
164 peak contamination is located at the shallow aquifer, where all CEs are detected, whereas
165 the plume outside the source zone is mainly composed of *cis*-DCE. DNAPL was detected at
166 the shallow aquifer of the south plume (MW-14 piezometer). The deep aquifer is also
167 contaminated in the north area, albeit CEs concentrations are significantly lower compared
168 to the shallow aquifer, whereas concentrations of CEs in the south are <500 µg/L and often
169 below the limit of quantification (LOQ). North (N.E.W.) and south (S.E.W.) exploitation wells
170 are located within the deep aquifer plumes. A schematic representation of the plumes, the
171 location of each of the exploitation wells, and the groundwater natural flow direction, are
172 depicted in Fig. S2. A network of about 100 sampling points was available for the study site
173 investigation and characterization (previous work, data not shown), from which 21 were
174 used for the present study (Fig. 1) and their constructive details are shown in Table S1. See
175 SI section 1.1 for more information on the study site.

176 *2.2. Collection of groundwater samples*

Groundwater samples were collected at different time points from different piezometers for i) assessing the intrinsic natural bioremediation potential by hydrogeochemical, microbiological and isotopic evidences; ii) executing treatability laboratory microcosms, and iii) monitoring the *in situ* bioremediation and B-ISCR pilot tests (Fig. 1). Groundwater sampling was performed with a peristaltic pump following the methodology described in Blázquez-Pallí et al. (2019a, 2019b), except that the *in situ* physicochemical parameters of groundwater (pH, temperature (T), electric conductivity (EC), dissolved oxygen (DO) and oxidation-reduction potential (ORP)) were measured with a Multiparametric Meter HI 98494 (Hanna Instruments). Absolute ORP measurements were then converted to Eh (relative to the reference standard hydrogen electrode, SHE). Groundwater samples were preserved with H_2SO_4 (pH<2) to prevent further transformation processes, except those destined for the establishment of microcosms and for molecular analyses, which were kept refrigerated until use.

2.3. Laboratory experiments

2.3.1. Microcosms to assess the bioremediation potential

The intrinsic bioremediation potential and the feasibility of bioremediation were assessed for both north and south source zones, and both shallow and deep aquifers. Six groundwater samples were collected in June 2022 from the following piezometers: MW-1 (north shallow aquifer), MW-2 (north deep aquifer), MW-16, MW-15 and MW-14 (south shallow aquifer) and MW-13 (south deep aquifer) (Fig. 1). From each of these samples, three different treatments were prepared, at least in duplicate: (1) control containing only groundwater, (2) groundwater with sodium lactate (3 mM), and (3) groundwater with a lecithin-based substrate (~3 mM). Microcosm experiments containing 70 mL of groundwater were established anaerobically in 100 mL glass serum bottles, and incubated at 25 ºC as described elsewhere (Blázquez-Pallí et al., 2019a). Liquid samples were obtained over time for the monitoring of physicochemical parameters (pH, T, EC, DO and Eh) and anions, whereas headspace samples were taken for the analysis of concentrations of CEs and ETH. Liquid samples from selected microcosm experiments were also collected for DNA extraction and further molecular analyses.

2.3.2.Microcosms to assess the B-ISCR potential

B-ISCR was assessed as an alternative treatment strategy for the north deep aquifer. Microcosm experiments were prepared with groundwater collected from piezometer MW-2 in January 2023 (Fig. 1). Four different treatments were established in duplicate: a control containing only groundwater, and three scenarios with groundwater, sodium lactate (3 mM), and sulfidized mZVI at concentrations of 0.04, 0.3 and 1.0 g mZVI/L, to consider a low dose, and the dose ranges that are typically recommended for field applications (Fu et al., 2014; Salom et al., 2023). All microcosms were prepared inside an anaerobic chamber, in borosilicate glass ISO bottles of 2,000 mL nominal volume, and contained 2,000 mL of sampled groundwater. They were incubated in the dark at ~17ºC under static conditions. Periodic sampling was performed for the measurement of physicochemical parameters (pH, T, EC, DO and Eh) and the analysis of concentrations of cations (Fe, Mn), CEs, and alkane and alkene gases from liquid samples.

2.3.3.Experiments to determine the isotope fractionation associated to reductive dechlorination

Given that the primary CE detected in groundwater at the site is *cis*-DCE, that PCE and TCE are present in relatively low concentrations outside the source zones, and that PCE reductive dechlorination often does not show significant carbon isotopic fractionation (εC) (Ojeda et al., 2020; Renpenning and Nijenhuis, 2016), the anaerobic biotic reductive dechlorination of *cis*-DCE was the selected transformation reaction for the determination of the site-specific εC. Eight parallel cultures amended with sodium lactate were prepared simultaneously, as described in section 2.3.1, with groundwater sampled on January 2023 from piezometer MW-1 (north shallow aquifer) (Fig. 1). Each microcosm was spiked with *cis*-DCE (160 µM, >97% purity, Sigma Aldrich, Merck), after removing all pre-existing volatile compounds by vaporization, and sacrificed with HNO_3 (pH<2) at different time points of *cis*-DCE degradation (0, 11, 17, 22, 48, 65, 65, 88%). A HNO_3-killed control containing groundwater and *cis*-DCE was prepared in duplicate and sampled periodically. Concentration and CSIA analyses for *cis*-DCE and VC were performed over time.

2.4. Implementation and monitoring of the in situ remediation pilot tests

Three *in situ* remediation pilot tests were implemented in selected locations of the site based on the results obtained in the laboratory experiments. Two bioremediation pilot tests were implemented around piezometers MW-1 (north shallow aquifer) and MW-16 (south shallow aquifer) (Fig. 1). In both cases, an aqueous solution of sodium lactate was used as amendment in two separate injection events at each pilot test. The third pilot test consisted in a B-ISCR treatment at the north deep aquifer and was implemented around piezometer MW-2 (Fig. 1). An aqueous solution of sodium lactate was injected at the first injection event in piezometer MW-2, and then it was combined with sulfidized mZVI for the last two injection events in piezometer MW-10. Considering MW-2 screened length, MW-10 piezometer was installed close to MW-2 with a shorter screen length to ensure some degree of monitoring capability between the two sampling points (Table S1). During the piezometer installation works, a complete hydraulic connection was evidenced between the two piezometers.

The three pilot tests lasted between 120 and 200 days, and the monitoring was performed every 20-30 days from a total of 21 sampling points (see Fig. 1). Further details can be found in SI section 1.2. Groundwater physicochemical field parameters (pH, T, EC, DO and Eh) were periodically measured *in situ* and groundwater samples were collected for the analysis of the concentrations of major ions, CEs, and alkane and alkene gases, and CSIA of CEs. Except for the concentration of CEs and alkane and alkene gases, with a higher frequency, all these analyses were performed only in groundwater samples collected at the beginning and at the end of each pilot test. In selected groundwater samples, DNA extraction and further molecular analyses were performed.

2.5. Analytical methods

Concentrations of CEs (PCE, TCE, *cis*-DCE and VC) were analysed from 500 µL headspace samples by gas chromatography (GC model 6890N, Agilent Technologies) coupled to a flame ionization detector (GC-FID) as described elsewhere (Martín-González et al., 2015), except that peak areas were quantified with the Chromeleon software 6.8 (Thermofisher). Samples from the B-ISCR microcosms and the monitoring of the *in situ* pilot

tests were analysed at an external laboratory by gas chromatography-mass spectrometry (GC-MS), according to the NEN-EN-ISO 10301 and NEN-EN-ISO 20595 standards.

Methane and ETH concentrations were analysed from 500 µL headspace samples using the same GC-FID described above, but equipped with a HP Plot Q column (30 m x 0.53 mm, 40 µm film thickness, Agilent Technologies). The oven, injector and detector temperatures were set at 150 °C, 250 °C and 260 °C, respectively. Run time lasted 7 min and the peak areas were quantified with the Chromeleon software 6.8 (Thermofisher). Samples from the B-ISCR microcosms and the monitoring of the *in situ* pilot tests were analysed at an external laboratory by GC-FID, following an internal method.

Concentration of anions (NO_3^-, NO_2^-, SO_4^{-2}, PO_4^{-2}, Cl^-) was analysed on a Dionex ICS-2000 ion chromatography system equipped with an IonPac AS18 anion-exchange column as described elsewhere (Trueba-Santiso et al., 2022). Groundwater samples from the monitoring of the *in situ* pilot tests were analysed at an external laboratory by liquid phase ion chromatography according to the ISO 10304-1 standard (SO_4^{-2}, Cl^-, Br^-), and by UV-vis spectrometry following the NEN-ISO 15923-1 standard (NO_3^-, NO_2^-, PO_4^{-2}).

Concentration of dissolved Mn and Fe was analysed at an external laboratory by inductively coupled plasma mass spectrometry (ICP-MS), following the NEN-EN-ISO 17294-2 standard.

For carbon isotope analysis of CEs, groundwater samples or liquid aliquots from the experiments were diluted as needed in ultrapure water into 20 mL vials filled to 10 mL final volume to adjust the concentration of the pollutants for subsequent isotope signature determination. Carbon isotope analyses were performed by headspace solid phase microextraction (HS-SPME) coupled to gas chromatography isotope ratio mass spectrometry (GC-IRMS), as detailed in the SI section 1.3. Samples were analysed in duplicate and obtained values were corrected by daily values of calibrated in-house CEs standards of known C isotope ratio, following the principle of identical treatment (Werner and Brand, 2001). All analyses had a one standard deviation (1σ) lower than 0.4‰.

The isotopic compositions of carbon from CEs in liquid samples are reported in delta notation ($\delta^{13}C$, in ‰), relative to the international standard VPDB (Vienna Pee Dee Belemnite) (Coplen, 1996), as follows

$$\delta^{13}C = \left(\frac{R_{sample}}{R_{std}} - 1\right) \quad (1)$$

where R_{sample} and R_{std} are the isotope ratios (i.e., $^{13}C/^{12}C$) of the sample and the standard, respectively (Elsner, 2010).

2.6. Isotope data evaluation

The carbon isotopic mass balance ($\delta^{13}C_{SUM}$) for CEs from groundwater samples from selected piezometers and from the laboratory experiments was calculated as reported elsewhere (Aeppli et al., 2010; Hunkeler et al., 1999), as follows

$$\delta^{13}C_{SUM} = x_{PCE} \cdot \delta^{13}C_{PCE} + x_{TCE} \cdot \delta^{13}C_{TCE} + x_{cis-DCE} \cdot \delta^{13}C_{cis-DCE} + x_{VC} \cdot \delta^{13}C_{VC} \quad (2)$$

where *x* is the molar fraction of each CE with respect to the total molar mass (sum of CEs for which $\delta^{13}C$ values were available) for each sample analysed. Provided that CEs are sequentially transformed via reductive dechlorination and this is the only active transformation pathway, $\delta^{13}C_{SUM}$ should remain constant as long as the contaminant source is the same, and VC (or the last CE considered in the isotope mass balance) is not further degraded (Aeppli et al., 2010; Hunkeler et al., 1999; Palau et al., 2014).

To determine the site-specific εC for the biotic reductive dechlorination of *cis*-DCE ($\varepsilon C_{cis\text{-}DCE}$), a modified version of the Rayleigh equation in the logarithmic form was used (Eq. 3), which defines the relationship between changes in the carbon isotopic composition of *cis*-DCE (R_t/R_0) with the extent of its biodegradation in laboratory experiments ($f=C_t/C_0$) (Coplen, 2011; Elsner, 2010).

$$\ln\left(\frac{R_t}{R_0}\right) = \ln\left(\frac{\delta^{13}C_t + 1}{\delta^{13}C_0 + 1}\right) = \varepsilon_C \cdot \ln(f) \quad (3)$$

R_t/R_0 can be expressed as $(\delta^{13}C_t+1)/(\delta^{13}C_0+1)$ according to $\delta^{13}C$ definition (Eq. 1). The $\varepsilon C_{cis\text{-}DCE}$, obtained from the slope of the linear regression (Eq. 3), can be used to quantify the extent of *cis*-DCE biodegradation (%D) in the field (Elsner, 2010). In this study, %D was

estimated for assessing the efficiency of the *in situ* pilot test, which is derived from the Rayleigh equation (Eq. 3), as follows

$$D\% = \left[1 - \left(\frac{\delta^{13}C_t + 1000}{\delta^{13}C_0 + 1000}\right)^{\frac{1000}{\varepsilon_C}}\right] \cdot 100 \qquad (4)$$

where εC is the isotopic fractionation, and $\delta^{13}C_0$ and $\delta^{13}C_t$ correspond to carbon isotopic composition prior to the start of the pilot tests and at the last sampling event for each pilot test, respectively.

Shifts in carbon isotope data ($\Delta\delta^{13}C$) were only considered to be significant for environmental samples when >2‰ (Hunkeler et al., 2008).

Errors given for $\varepsilon C_{cis\text{-DCE}}$, and for $\delta^{13}C_{SUM}$ and %D, correspond to the 95% confidence interval (CI) of the linear regression in the Rayleigh plot, and to the uncertainty calculated by error propagation, respectively.

2.7. DNA extraction, qPCR and 16S rRNA gene high-throughput sequencing

The microbiota present in liquid samples from the bioremediation microcosms was separated by filtration through a nitrocellulose membrane (0.22 µm), while cell harvesting from groundwater samples collected during the monitoring of the *in situ* pilot tests was carried out by filtration through Sterivex™ filters (0.22 µm). In all cases, total DNA was obtained using the commercial DNAeasy PowerSoil kit (Qiagen), and the quality and quantity of the obtained DNA was determined using Nanodrop. For the DNA obtained from the microcosms, quantitative PCR (qPCR) assays were performed to quantify the abundance of *Dehalogenimonas* (*Dhg*) 16S rRNA and *Dhc* 16S rRNA gene copies, the VC reductive dehalogenase functional genes *vcrA* and *bvcA*, and the TCE reductive dehalogenase functional gene *tceA*. The specific primer sets and the qPCR amplification programs used are described elsewhere (Behrens et al., 2008; Krzmarzick et al., 2012; Şimşir et al., 2017; Yan et al., 2009). Biomarker quantification via qPCR was carried out on a StepOne Plus system (Applied Biosystems) in 20 µL total reaction volumes. Calibration curves were prepared using 10-fold standard recombinant plasmid dilutions, containing the insert with the corresponding marker/primer, as the reference standard. All qPCR assays had an amplification efficiency that ranged from 87.8 to 126.2% and a slope ranging from -

347 3.9 to -2.8. For the DNA obtained from groundwater samples, *Dhc* 16S rRNA was the only
348 targeted biomarker to be quantified through qPCR as described above. In addition, high-
349 throughput sequencing of 16S rRNA gene libraries was performed on four groundwater
350 samples to analyse the structure of the bacterial community and determine how it is
351 affected by the treatments applied in the two bioremediation pilot tests.

352 **3. Results and discussion**

353 *3.1. Lines of evidence for natural CEs attenuation*

354 Groundwater samples collected at the two sampling campaigns performed for assessing the
355 natural bioremediation potential (June and December 2022, Table S2 and S3, respectively)
356 presented similar physicochemical conditions: circumneutral pH, EC typical of continental
357 groundwater (Custodio and Llamas, 1983), and Eh values between +55 and +204 mV,
358 except MW-2 in June 2022 (north deep aquifer), which evidenced a pH of 10.1 and Eh of -
359 83.2 mV (Table S2). Content of native potential electron acceptors varied among samples,
360 but both shallow and deep aquifer natural conditions reflected nitrate- to sulphate-reducing
361 conditions (Table S2 and S3), which would be appropriate for PCE, TCE and *cis*-DCE
362 reductive dechlorination (Aulenta et al., 2007; Blázquez-Pallí et al., 2019b; Bradley, 2003;
363 Elsner and Hofstetter, 2011; van der Zaan et al., 2010; Wiedemeier et al., 1998). Chloride
364 concentrations were directly proportional to the total CEs concentration (Table S2 and S3),
365 suggesting chloride release after CEs natural attenuation.

366 In terms of the distribution of dissolved CEs and ETH, PCE and *cis*-DCE predominated in
367 the north-derived groundwater samples; TCE and *cis*-DCE were the main CEs in the south-
368 derived samples, and VC and ETH were detected in almost all piezometers (Fig. 2, Table
369 S2 and S3). The molar fraction distribution and the presence of VC and ETH across the site
370 agrees with the above-mentioned hydrochemical evidences of natural attenuation.

371 The isotopic results, including $\delta^{13}C$ of each CE and the isotopic mass balance ($\delta^{13}C_{SUM}$, Eq.
372 2), are shown in Table S4 and Fig. 3A and B. At the north deep aquifer (MW-2), the
373 individual isotopic results for each CE suggest significant biodegradation of PCE and TCE
374 but not of *cis*-DCE, which would accumulate in the deep aquifer. This agrees with the
375 $\delta^{13}C_{SUM}$ value (-20.7‰), being similar to that of the original source at the north plume (-

21.7‰, SI section 1.4). In contrast, $\delta^{13}C_{SUM}$ at the north shallow aquifer (MW-1, MW-3 and MW-4) deviated significantly from the original source isotopic composition, especially in MW-1 (-15.2‰) and MW-3 (-16.2‰). These results, together with the individual $\delta^{13}C$ values for each CE, point to further *cis*-DCE degradation in these piezometers, which is consistent with the CEs molar fractions (Fig. 2). They also suggest the occurrence of some degree of VC degradation to ETH, but the fact that the $\delta^{13}C_{VC}$ value was very close to the $\delta^{13}C_{SUM}$ value indicates that VC biodegradation was not significant, and VC likely accumulated in the shallow aquifer (Table S4). At the south shallow aquifer, the $\delta^{13}C_{SUM}$ for MW-16 (-22.6‰) is consistent with the isotopic composition of the original source at the south plume (-24.4‰, SI section 1.4), pointing to a significant biodegradation of PCE and TCE, but not *cis*-DCE or VC. In the case of MW-17, the degradation would go beyond *cis*-DCE, although VC degradation was not very significant. Finally, the $\delta^{13}C_{SUM}$ value of MW-18 (7.0‰) is significantly different from that of MW-16 and MW-17, and from the original source. This is a sample in which practically only *cis*-DCE remained (96% molar fraction), with a $\delta^{13}C_{cis\text{-DCE}}$ value indicative of a very advanced state of biodegradation of PCE, TCE and *cis*-DCE (Fig. 3A and B).

3.2. Assessment of the feasibility of in situ remediation treatments in laboratory experiments

3.2.1. Study of the intrinsic bioremediation potential of the site

Both amendments used for assessing the intrinsic bioremediation potential and the feasibility of bioremediation (lactate and lecithin) induced changes in the DO content compared to the unamended controls, resulting in lower DO levels ($DO_{lactate} < DO_{lecithin}$, Fig. S3A). Compared to the control, lactate did not promote a significant pH change, whereas lecithin lowered it to pH~5-6 (Fig. S4A). It is remarkable, on the contrary, that both amendments led to a pH decrease for the more alkaline groundwater of the north deep aquifer (MW-2, Fig. S4B). Lactate promoted an increase in EC and a decrease in Eh, while lecithin increased Eh (Fig. S3). These patterns were observed across all microcosms.

Time-course of CEs concentrations evidenced that lactate promoted the full dechlorination of CEs to ETH in groundwater from MW-1, MW-16 and MW-15 piezometers (shallow aquifer), with VC starting to be transformed to ETH within the first

80 days (Fig. 4). In MW-1 and MW-16 microcosms, this CEs sequential dechlorination to ETH resulted in an increase in gene copies of OHRB capable of full dechlorination of CEs to ETH (*Dhc* and *Dhg*), and in the analysed reductive dehalogenase genes (*tceA*, *vcrA*, *bvcA*) (Fig. 5A and B). This fact indicates that CEs biodegradation was coupled to *Dhc* and *Dhg* growth.

The unamended microcosms, which account for natural attenuation processes, fully converted PCE to *cis*-DCE within 30 days, and VC started to increase by day 80, but ETH was not detected within the first 110 days (Fig. S5). The CEs transformation rates were lower than in the lactate-amended microcosms, but similar to the lecithin-amended microcosms, which stalled at *cis*-DCE probably due to the low pH (≤6) (Fig. S4A, S5) (Adrian and Löffler, 2016; Yang et al., 2017a) or to the accumulation of secondary products (e.g., volatile fatty acids by-products of the fermentation of the lecithin-based amendment) (Aulenta et al., 2007).

The addition of lactate did not lead to the reductive dechlorination of CEs in MW-2, MW-14 and MW-13 (Fig. S6). In MW-2 microcosms (north deep aquifer), qPCR results did not show growth in any of the biomarker gene copies (Fig. 5C), probably due to the alkaline pH (Adrian and Löffler, 2016) (Fig. S4B). For MW-14, qPCR evidenced a moderately-high abundance of biomarkers but no growth (Fig. 5D), which would agree with the inhibition of OHRB due to the high CEs concentrations (detection of DNAPL in this piezometer, Table S2) (National Research Council, 1999; Philips et al., 2013). CEs concentrations in groundwater from the south deep aquifer (MW-13) were close to the LOQ of the analytical method (Table S2), so the results from the corresponding microcosms are not presented due to the analytical uncertainty and the little representativeness of the site contamination. However, a moderately-high abundance of the selected biomarkers was detected at the end of the MW-13 experiment (Fig. 5E), which would suggest potential for CEs biotic reductive dechlorination for the south deep aquifer.

Therefore, the treatability microcosms demonstrated that biotic reductive dechlorination was enhanced in both north and south shallow aquifers (as long as there are no inhibition issues), and that OHRB were moderately-high abundant in the south deep

aquifer as well. However, no evidence of biodegradation potential was obtained for the north deep aquifer (MW-2), which led to assess the feasibility of an alternative remediation strategy based on B-ISCR for this aquifer.

3.2.2. Study of the B-ISCR potential

The B-ISCR experiments performed with groundwater from piezometer MW-2 to investigate an alternative treatment strategy for the north deep aquifer resulted in an increase of DO inversely proportional to the sulfidized mZVI doses: $DO_0 > DO_{0.04} > DO_{0.3} > DO_{1.0}$, where the subindexes refer to the mZVI dose used (in g mZVI/L), and DO_0 refers to the control microcosm (Fig. S7A). On the contrary, EC was impacted in a directly proportional manner by the amendment doses: $EC_0 << EC_{0.04} < EC_{0.3} < EC_{1.0}$ (Fig. S7B). With regards to pH, the higher the dose of sulfidized mZVI, the more circumneutral the pH was (Fig. S7C). The Eh showed an increasing trend over time and did not differ significantly among the prepared microcosms (Fig. S7D).

Time-course of CEs and ETH content showed that the B-ISCR treatment (lactate plus sulfidized mZVI amendment) promoted a higher transformation of the contaminants compared to the unamended control (Fig. S8), but also compared to the lactate-amended microcosm (Fig. S6B). Accordingly, Cl^- concentration slightly increased with the progress of the experiment (Fig. S9A), especially in the experiments with higher mZVI doses. Observed trends for dissolved total Fe (Fig. S9B) were consistent with initial ZVI corrosion (the higher the ZVI dose, the higher the Fe release), likely followed by precipitation of minerals, agreeing with the visual observations. Indeed, precipitation of ferrous hydroxides and further oxidation to magnetite, siderite or calcium carbonate are thought to significantly decrease ZVI reactivity (Prommer et al., 2008). Lastly, dissolved Mn did not change significantly (Fig. S9B). Even though the B-ISCR experiments were monitored for a short period, the obtained results demonstrate the potential of the combined biotic and abiotic reductive dechlorination treatment.

3.3. Site-specific εC for cis-DCE biodegradation

Killed controls showed no degradation of *cis*-DCE, since both concentration (Fig. S10) and $\delta^{13}C_{cis\text{-DCE}}$ (Fig. 6A) remained constant throughout the experiment (15472 ± 34 µg/L, -27.4 ±

0.3‰, n=3). In contrast, *cis*-DCE consumption and VC formation was observed in the active microcosms (Fig. S10), coupled with an increase in $\delta^{13}C_{cis\text{-DCE}}$ from −27.08 ± 0.03 to +39.6 ± 0.4‰ after 88% *cis*-DCE transformation (Fig. 6A). The produced VC showed an initially ^{13}C-depleted $\delta^{13}C$ with respect to the initial $\delta^{13}C_{cis\text{-DCE}}$, in accordance with a normal isotopic effect, and shifted toward more ^{13}C-enriched values during the course of reaction (Fig. 6A). The isotopic mass balance ($\delta^{13}C_{SUM}$, Eq. 2) is consistent with the initial $\delta^{13}C_{cis\text{-DCE}}$ (-27.08 ± 0.03‰) and with that of the control experiment (horizontal dashed line in Fig. 6A), remaining constant throughout the experiment except for the final point ($\delta^{13}C_{SUM}$ = -13.0 ± 0.4‰), indicating that VC was also being degraded from that moment on. The site-specific *cis*-DCE carbon isotope fractionation was determined by the Rayleigh approach as $\varepsilon C_{cis\text{-DCE}}$ = −31.8 ± 2.9‰ (Fig. 6B), a value that falls within the previously reported range for *cis*-DCE reductive dechlorination (from -31 to -15‰, Renpenning and Nijenhuis (2016), Ojeda et al., (2020)), and is sufficiently large to be used as a robust indicator for quantifying the efficiency of bioremediation (%D) in the field.

3.4. Performance evaluation of the in situ remediation pilot tests

3.4.1. Hydrochemistry changes induced by the amendment injection

In the bioremediation pilot test at the south shallow aquifer, the two lactate injections in piezometers MW-17 and MW-16 promoted the achievement of sulphate-reduction to methanogenic conditions which are optimal for reductive dechlorination (Wiedemeier et al., 1998) (Table S3, Fig. S11). The pH remained circumneutral, whereas significant increases in EC were observed after the second injection in both injection piezometers.

In the bioremediation pilot test at the north shallow aquifer, complete anoxic conditions were not achieved after the two lactate injections in MW-1, as evidenced by the detection of sulphate (>20 mg/L) and DO (>0.5 mg/L) at the end of the treatment (Table S3, Fig. S12). The pH and EC followed the same trend as the other bioremediation pilot test, with significant increases in EC in the injection piezometer after each injection event.

For the B-ISCR pilot test at the north deep aquifer (injection, first in piezometer MW-2, and thereafter in piezometer MW-10), the increase of methane concentration in both

494 piezometers, and dissolved Fe and Mn in MW-10 (Table S3) suggests that a shift
495 towards more reducing conditions occurred. Accordingly, oxygen was depleted (DO
496 <0.5 mg/L) most of the days (Fig. S13). EC also increased after the second and the
497 third injections, whereas the pH remained mainly circumneutral. The effect of the
498 second and third injection in MW-10 is evident in the EC of both MW-2 and MW-10
499 piezometers, reflecting their hydraulic connectivity.

500 For the three *in situ* pilot tests, in all injection piezometers except MW-17, the
501 concentration of chloride increased after the treatment (Table S3), indicating reductive
502 dechlorination of CEs. The changes in the *in situ* physicochemical parameters on the
503 rest of the monitoring points for each pilot test (data not shown, see piezometers in Fig.
504 1 and Table S1), suggest that the radius of influence of the injections (i.e., amendment
505 dispersion) was bigger in the south shallow and north deep aquifers, than in the north
506 shallow aquifer, probably due to the lithology of the area and a greater presence of
507 clays. This could also explain the observed difficulty in promoting and maintaining
508 reducing conditions during the bioremediation pilot test at the north shallow aquifer (Fig.
509 S12).

510 *3.4.2.Enhanced degradation of CEs at the monitoring piezometers*

511 Prior to the lactate injections, *cis*-DCE was the main CEs dissolved in groundwater in
512 both areas where the two bioremediation pilot tests were implemented (north and south
513 shallow aquifers). After the lactate injections in the south pilot test, conversion of *cis*-
514 DCE to VC and ETH was observed at the injection piezometers MW-16 and MW-17;
515 albeit the biodegradation process seemed more efficient in MW-16 (Fig. 7A1 and A2).
516 However, throughout the pilot test, increases in PCE and TCE concentrations were
517 detected in the three monitoring piezometers (including also MW-18) (Fig. 7A1, A2, and
518 A3), probably due to back diffusion of contaminants from secondary sources.
519 Consequently, the concentration of *cis*-DCE, VC and ETH also increased.

520 In the north bioremediation pilot test (MW-1, MW-3 and MW-4), conversion of *cis*-DCE
521 to CV and ETH was also observed (Fig. 7B1, B2, and B3), although ETH was produced
522 at a lower concentration than in the south bioremediation pilot test. Therefore, an

523 evident sequential transformation of *cis*-DCE to VC to ETH was not observed, in
524 contrast to the results obtained in the treatability microcosms (Fig. 4A, Fig. 6). Thus,
525 field records could suggest the occurrence of low-efficiency reductive dechlorination
526 reactions. Increases in PCE and TCE concentrations, probably related to releases by
527 back diffusion, were also detected in this pilot test, which probably contributed to the
528 notable variation of *cis*-DCE concentrations over time.

529 Time-course of CEs and ETH concentrations at the two injection piezometers MW-2
530 and MW-10 during the B-ISCR pilot test at the north deep aquifer is shown in Fig. 7C.
531 The first lactate injection in MW-2 induced some degree of biotic reductive
532 dechlorination at this piezometer, resulting in complete PCE and TCE transformation to
533 *cis*-DCE within 75 days (Fig. 7C1). It is likely that the injected lactate also reached MW-
534 10, given their hydraulic connectivity and the *cis*-DCE detected prior to the second
535 injection (Fig. 7C2). Such behaviour points to the presence of OHRB in the north deep
536 aquifer, and contradicts the results obtained in the lactate-amended microcosms for this
537 piezometer (Fig. S6B). It is possible that the groundwater sample used for those
538 experiments were not representative of the deep aquifer conditions, since it was
539 collected at a time where boreholes had been recently executed in the area.
540 Approximately 125 days after the first injection of a combined lactate and sulfidized
541 mZVI solution in MW-10, a similar trend in CEs evolution, with transient *cis*-DCE
542 accumulation and ETH production, was observed in both MW-10 and MW-2 (Fig. 7C).
543 Again, the effect of the injection in one piezometer is detected in the other one, likely
544 because all the amendment injections reached both piezometers given the hydraulic
545 connectivity between them. Besides transient *cis*-DCE accumulation, VC was also
546 detected, but at concentrations <1000 µg/L. This fact suggests that both biotic
547 (hydrogenolysis, VC as intermediate) and abiotic (mainly as β-elimination, VC is usually
548 bypassed) reductive CEs dechlorination processes were enhanced with the combined
549 B-ISCR strategy at the north deep aquifer. The possible co-occurrence of both
550 processes could not be confirmed, since typical non-chlorinated intermediates for the
551 ZVI-induced reductive β-elimination process, such as dichloroacetylene,
552 chloroacetylene and acetylene, were not analysed in this study. Nevertheless, these

intermediates are rarely reported for the ZVI-treated field studies because of their challenging quantification related to their quick volatilization (Nunez Garcia et al., 2020).

3.4.3.Changes in the native microbial community induced by the bioremediation pilot tests

The *Dhc* 16S rRNA gene copy numbers increased almost two orders of magnitude in the injection piezometers (MW-1 at the north shallow aquifer, and MW-16 and MW-17 at the south shallow aquifer) in the two bioremediation pilot tests (Fig. 8). On the contrary, the monitoring point MW-4, located 7-8 m from the injection piezometer MW-1, evidenced a decrease in *Dhc* 16S rRNA gene copies of one order of magnitude. These results demonstrate the efficiency of the injections of lactate as electron donor and carbon source to promote *Dhc* growth.

Massive sequencing of the 16S rRNA region in groundwater collected from the injection piezometers MW-1 (north shallow aquifer) and MW-16 (south shallow aquifer) prior (T0) and after (TF) the pilot tests evidenced a dramatic shift in the structure of the bacterial communities caused by lactate injection (Table S5 and S6). Using the OTU label, the Jaccard similarity coefficient, which considers only the presence or absence of a population and not its relative abundance, was computed for high- (>1%), low-abundance (<1%), and all OTUs, to estimate the similarity of the microbial communities at piezometers MW-1 and MW-16 at T0 and TF. The Jaccard index was calculated between T0 and TF of each piezometer to assess whether microbial communities remained similar after lactate injections, but also between the two piezometers at each sampling time to evaluate whether community shifts followed a similar trend across the site. The Jaccard index calculations suggest that lactate injections considerably changed the community composition at each piezometer (T0 vs. TF), and increased the similarity of the microbial populations between the two studied piezometers (MW-1 vs. MW-16, Table S7). The injections also resulted in a clear decrease in microbial diversity from T0 to TF, as reflected by the Shannon Diversity index, which decreased from 4.9 to 4.1 in MW-1, and from 6.5 to 3.7 in MW-16. Prior to lactate injection at the north shallow aquifer (MW-1), members of the *Comamonadaceae* family predominated (Table S5), which are characterized by great metabolic versatility, with representatives capable

583 of aerobically degrading organic contaminants (Willems, 2014; Yi et al., 2022). After the
584 treatment, these populations were completely displaced by fermenting bacteria, typical
585 of anaerobic environments with relatively abundant organic carbon sources (Blázquez-
586 Pallí et al., 2019b). Some of them, such as *Bacteroides* (OTU1) and *Syntrophomonas*
587 (OTU11), are typical of methanogenic environments (McInerney et al., 1981;
588 Tukanghan et al., 2021). It is also worth noticing the increase in *Desulfitobacterium*, with
589 an abundance >13% after the treatment (Table S8), since some strains of this genus
590 are capable of reductive dechlorination (Futagami and Furukawa, 2016). At the south
591 shallow aquifer (MW-16), the most abundant populations before the lactate injections
592 were also linked to aerobic respiration; indeed, some belong to uncultivated genera,
593 and some are chemolithotrophs, such as *Gallionella* (OTU12) (Table S6), typical of
594 environments that are poor in organic matter (Hanert, 2006). As occurred in the north
595 bioremediation pilot test, a predominance of fermenters, especially *Bacteroides* (OTU1)*,*
596 was detected in the injection piezometer after the treatment (Table S6).

597 An exhaustive search was carried out for genera associated with reductive
598 dechlorination (Adrian and Löffler, 2016) in all four analysed samples and, at least, *Dhc*,
599 *Dhg*, *Geobacter*, *Dehalobacter*, *Desulfitobacterium* and *Sulfurospirillum* were detected
600 (Table S8). Only *Dhc* and *Desulfitobacterium* evidenced an increase in relative
601 abundance after the injections in both piezometers. In MW-1, *Desulfitobacterium*
602 showed the greatest increase (13.9%), while *Dhc* changed from representing 0.007% of
603 the community at T0 to 0.03% at TF. In MW-16, *Dhc* increased from 0% to 0.3%.
604 Comparatively, *Dhc* relative abundance is low, which is expected from their low natural
605 abundance, even at CEs polluted sites (Adrian and Löffler, 2016). Regarding the other
606 OHRB, *Dhg*, *Geobacter* and *Dehalobacter* only increased their relative abundance in
607 MW-16, while *Sulfurospirillum* only increased in MW-1, further proving the little similarity
608 in community composition (Table S8). These results would also support the
609 observations that reductive dechlorination conditions were harder to maintain at the
610 north shallow aquifer (MW-1). Lastly, although the correlation between 16S rRNA
611 concentration and growth rate can be, in some cases, not straightforward (Blazewicz et
612 al., 2013), the increase in the relative abundance of *Dhc* agrees well with the increase

in absolute numbers of *Dhc* 16S rRNA gene copies (Fig. 8). Similarly, *Dhg* 16S rRNA gene copies were not used as a biomarker during the bioremediation pilot tests, but the observed increase in their relative abundance at MW-16 (Table S8) would also agree with the growth observed in the lactate-amended laboratory microcosms after complete reductive dechlorination (Fig. 5).

3.4.4.Efficiency of the pilot tests based on an isotopic evaluation

In general, when comparing isotopic results corresponding to T0 (prior to the start of the pilot test, Table S4) and TF (at the last sampling event, Table S9) in all pilot tests, a trend towards the enrichment in ^{13}C in $\delta^{13}C$ values of all CEs was observed (Fig. 3A and C). In the bioremediation pilot test implemented at the south shallow aquifer, compared to T0, the molar fraction of PCE and, especially, TCE increased at TF in the three monitoring piezometers (Fig. 3B and D). $\delta^{13}C$ data confirmed the occurrence of arrivals of non-degraded PCE and TCE, with $\delta^{13}C$ for both compounds similar to the original source at the south plume (Fig. 3C). Accordingly, $\delta^{13}C$ results showed that the lactate-enhanced bioremediation was only evident in MW-16, probably due to the masking effect of contributions of non-degraded CEs in the other two monitoring piezometers (MW-17 and MW-18). A ^{13}C enrichment was observed in MW-16 for *cis*-DCE and VC, with final $\delta^{13}C$ values more positive than that of TCE, confirming *cis*-DCE and VC degradation (Table S9). These results, together with the results of $\delta^{13}C_{SUM}$ (Fig. 3D), confirmed that reductive dechlorination clearly passed beyond VC in this piezometer, contrary to what was observed prior to the lactate injections (Fig. 3B). The degradation of VC was further corroborated in all three piezometers by the detection of ETH (Fig. 7A). Although the shift in $\delta^{13}C_{cis\text{-DCE}}$ between T0 and TF in MW-16 was $\Delta\delta^{13}C$ >2‰, the efficiency of the bioremediation pilot test for *cis*-DCE (%D, Eq. 4) could not be reliably estimated since PCE and TCE had not been completely consumed at TF. This is because $\delta^{13}C_{cis\text{-DCE}}$ is affected not only by *cis*-DCE degradation, but also by its formation from TCE.

In the bioremediation pilot test performed in the north shallow aquifer (piezometers MW-1, MW-3, and MW-4), CEs molar fractions were similar before and after the treatment,

642 except with slight decreases in PCE and TCE fractions and increases in *cis*-DCE and
643 VC fractions (Fig. 3B and D). $\delta^{13}C$ values evidenced an enrichment in the heavy isotope
644 for some CEs at TF (Fig. 3C), indicating an advanced degradation in the reductive
645 dechlorination chain, with VC degradation especially occurring in the injection
646 piezometer MW-1. Nevertheless, $\delta^{13}C_{SUM}$ remained practically identical to that of T0
647 (Fig. 3). This could be explained by the arrival of non-degraded PCE and TCE, which
648 was also hinted in the time-course of CEs concentrations (Fig. 7B). As occurred for the
649 bioremediation pilot test at the south shallow aquifer, its efficiency could not be
650 quantified for *cis*-DCE, since complete consumption of PCE and TCE did not occur. It
651 was possible, however, to roughly estimate %D for PCE using the wide range of εC
652 values associated with the reductive dechlorination of PCE reported in the literature (-
653 0.5 to -25.3‰, Adrian and Löffler (2016)). The calculation resulted in a wide %D range
654 for lactate-enhanced PCE biodegradation, between 14 and 99% (Table S10). A more
655 precise estimation would require the determination of site-specific εC_{PCE} for this aquifer.

656 Regarding the B-ISCR pilot test implemented at the north deep aquifer, the isotopic
657 results showed that the treatment effect was evident in both injection piezometers (MW-
658 2 and MW-10). At the end of the monitoring period (62 days after the third injection),
659 besides the complete consumption of PCE and TCE, and the detection of VC and ETH
660 (Fig. 7C1 and C2), a significant decrease and increase in the molar fractions of *cis*-DCE
661 and VC, respectively, was observed compared to T0. The isotopic compositions of *cis*-
662 DCE and VC also showed a high ^{13}C enrichment in both injection piezometers (Fig. 3C).
663 These results confirmed degradation of both *cis*-DCE and VC. The significant change in
664 $\delta^{13}C_{SUM}$ in both piezometers (from -20.7‰ to +30.0‰ in MW-2, and from -20.6‰ to
665 +6.2‰ in MW-10, Fig. 3B and D), confirmed that the reductive dechlorination went
666 beyond VC. It should be noted that the value of $\delta^{13}C_{SUM}$ for MW-10 at TF, marked in
667 salmon in Fig. 3D, presents greater uncertainty because the contribution of $\delta^{13}C_{VC}$ in
668 $\delta^{13}C_{SUM}$, which could be significant given the molar fraction of VC, was not considered
669 (Table S9). Nevertheless, this deviation of the isotopic mass balance could also be
670 indicative of the co-occurrence of both lactate-enhanced biotic and sulfidized mZVI-
671 mediated abiotic CEs reductive dechlorination, as discussed in the previous section.

672 The complete consumption of PCE and TCE allows estimating the efficiency of the B-
673 ISCR pilot test in terms of *cis*-DCE transformation extent. Assuming unique contribution
674 from lactate-enhanced *cis*-DCE biodegradation, %D at the end of the B-ISCR pilot test
675 was estimated to be 78 ± 7% and 72 ± 7% in MW-2 and MW-10 piezometers,
676 respectively (Table S10), using the site-specific εC for *cis*-DCE determined in this study
677 ($\varepsilon C_{cis\text{-DCE}}$ = −31.8 ± 2.9‰). This efficiency estimation could also be performed assuming
678 unique contribution from sulfidized mZVI-mediated abiotic *cis*-DCE reductive
679 dechlorination, by using isotopic fractionations previously reported for *cis*-DCE reductive
680 dechlorination with ZVI, which ranged from -6.9‰ to -21.7‰ (Audí-Miró et al., 2013;
681 Elsner et al., 2008; VanStone et al., 2004). The calculation resulted in higher extents of
682 *cis*-DCE transformation, ranging between 89% and 99.9% for MW-2 and between
683 84.3% and 99.7% for MW-10. A multi-element CSIA approach would allow estimating
684 contributions of both reductive dechlorination processes for a more precise
685 quantification of the treatment efficiency, given that different C-Cl isotopic trends are, in
686 some cases, expected for both processes for *cis*-DCE (Ojeda et al., 2020). In any case,
687 carbon CSIA evidenced the successful performance of the B-ISCR pilot test, with an
688 efficiency higher than 70% for *cis*-DCE.

689 **4. Conclusions**

690 The present study used a multi-method assessment approach to design and select the optimal
691 full-scale bioremediation treatment at a multi-focus site in the north of the Iberian Peninsula
692 where both shallow and deep aquifers are contaminated by CEs. To adequately design the
693 research approach by means of laboratory and *in situ* pilot tests, it was necessary to understand
694 the conceptual site model for such a complex contaminated aquifer, which was improved in
695 previous works through a vast hydrogeological site investigation. The integrative methodology
696 used in this study included a hydrogeochemical and isotopic ($\delta^{13}C$) groundwater
697 characterization, and treatability laboratory microcosms that evaluated the intrinsic degradation
698 potential of the site, the presence of key biomarkers, as well as the feasibility of the proposed
699 bioremediation treatments. The hydrogeochemical and isotopic site characterization evidenced
700 natural attenuation of CEs at both north and south plumes. Microcosm experiments provided
701 evidence that, for both north and south shallow aquifers, full transformation of CEs to ETH can

be achieved with the addition of lactate. In these experiments, the sequential dechlorination of PCE to ETH was coupled to the growth of *Dhc* and *Dhg* and the increase in the gene copies of the reductive dehalogenases *tceA*, *vcrA* and *bvcA*. For the north deep aquifer, the lines of evidence gathered in the microcosm experiments evidenced that a combined biotic and abiotic reductive dechlorination (B-ISCR) can be a successful alternative for this aquifer through the addition of lactate and sulfidized mZVI.

Based on the results of the laboratory experiments, three *in situ* pilot tests were designed and implemented at this site, achieving in most cases full dechlorination to ETH, as evidenced by hydrochemical and molecular analyses, and the calculation of carbon isotope-mass balances. Full CEs dechlorination was accompanied by a change in the microbial populations from aerobic to fermenting bacteria. It is likely that the efficiency of the treatments was impacted by the hydrodynamics of the aquifers, which probably affected the amendment distribution; the contribution of non-degraded CEs due to back diffusion from secondary sources (confirmed by isotope data), and the presence of high CEs concentrations (confirmed in the laboratory microcosms prepared with groundwater derived from a piezometer with DNAPL). In the B-ISCR pilot test that combined the injection of lactate and sulfidized mZVI, both biotic and abiotic pathways contributed to the production of ETH. These results demonstrate that the use of sulfidized mZVI can enhance anaerobic biostimulation treatments with lactate.

Therefore, the integrated methodology followed in this study was a useful tool to improve the conceptual site model and determine that lactate-enhanced bioremediation is a valid strategy for the full-scale remediation of both impacted aquifers at this multi-focus complex site, and that it could be improved with sulfidized mZVI in the potential instances where biodegradation alone was not efficient or absent, preventing CEs further migration towards the nearby exploitation wells. These results emphasize the benefits of this integrative approach to support decision-making in the implementation and development of CEs bioremediation strategies at complex multi-focus and multi-polluted sites.

Acknowledgements

This research was supported by the projects PID2022-138929OB-I00 and PID2022-139911OB-C4-1, both funded by MCIN/AEI/10.13039/501100011033 and by ERDF A way of making Europe. This work was also supported by the Basque Water Agency (Agencia Vasca del Agua) through a public tender. We thank Foix Soler, Pedro Yáñez, Jon Burgos, Irene Janices and Arnau Puig for their contribution throughout the whole project; and Dr. Jesica M. Soder-Walz, Dani Salom, and the Scientific and Technological Centers of the University of Barcelona (CCiT-UB) for their excellent technical assistance.

740 **References**

741 Abe, Y., Aravena, R., Zopfi, J., Parker, B., Hunkeler, D., 2009. Evaluating the fate of chlorinated
742 ethenes in streambed sediments by combining stable isotope, geochemical and microbial
743 methods. J. Contam. Hydrol. 107, 10–21. https://doi.org/10.1016/j.jconhyd.2009.03.002

744 Adrian, L., Löffler, F.E., 2016. Organohalide-Respiring Bacteria, Organohalide-Respiring
745 Bacteria. Springer Berlin Heidelberg, Berlin, Heidelberg. https://doi.org/10.1007/978-3-
746 662-49875-0

747 Aelion, C.M., Höhener, P., Hunkeler, D., Aravena, R., 2009. Environmental Isotopes in
748 Bioremediation and Biodegradation. CRC Press, Boca Raton.
749 https://doi.org/10.1159/000076616

750 Aeppli, C., Hofstetter, T.B., Amaral, H.I.F., Kipfer, R., Schwarzenbach, R.P., Berg, M., 2010.
751 Quantifying in situ transformation rates of chlorinated ethenes by combining compound-
752 specific stable isotope analysis, groundwater dating, and carbon isotope mass balances.
753 Environ. Sci. Technol. 44, 3705–3711. https://doi.org/10.1021/es903895b

754 Arnold, W.A., Roberts, A.L., 2000. Pathways and Kinetics of Chlorinated Ethylene and
755 Chlorinated Acetylene Reaction with Fe(0) Particles. Environ. Sci. Technol. 34, 1794–
756 1805. https://doi.org/10.1021/es990884q

757 Atashgahi, S., Lu, Y., Smidt, H., 2016. Overview of known organohalide-respiring bacteria-
758 phylogenetic diversity and environmental distribution, in: Adrian, L., Löffler, F.E. (Eds.),
759 Organohalide-Respiring Bacteria. Springer, Berlin, Heidelberg, pp. 63–105.
760 https://doi.org/10.1007/978-3-662-49875-0_5

761 ATSDR, 2022. Substance Priority List [WWW Document]. U.S Public Heal. Serv. Agency Toxic
762 Subst. Dis. Regist. URL https://www.atsdr.cdc.gov/spl/#2022spl (accessed 1.2.24).

763 Audí-Miró, C., Cretnik, S., Otero, N., Palau, J., Shouakar-Stash, O., Soler, A., Elsner, M., 2013.
764 Cl and C isotope analysis to assess the effectiveness of chlorinated ethene degradation by
765 zero-valent iron: Evidence from dual element and product isotope values. Appl.
766 Geochemistry 32, 175–183. https://doi.org/10.1016/j.apgeochem.2012.08.025

767 Aulenta, F., Pera, A., Rossetti, S., Petrangeli Papini, M., Majone, M., 2007. Relevance of side

768 reactions in anaerobic reductive dechlorination microcosms amended with different
769 electron donors. Water Res. 41, 27–38. https://doi.org/10.1016/j.watres.2006.09.019

770 Badin, A., Broholm, M.M., Jacobsen, C.S., Palau, J., Dennis, P., Hunkeler, D., 2016.
771 Identification of abiotic and biotic reductive dechlorination in a chlorinated ethene plume
772 after thermal source remediation by means of isotopic and molecular biology tools. J.
773 Contam. Hydrol. 192, 1–19. https://doi.org/10.1016/j.jconhyd.2016.05.003

774 Behrens, S., Azizian, M.F., McMurdie, P.J., Sabalowsky, A., Dolan, M.E., Semprini, L.,
775 Spormann, A.M., 2008. Monitoring Abundance and Expression of " Dehalococcoides "
776 Species Chloroethene-Reductive Dehalogenases in a Tetrachloroethene-Dechlorinating
777 Flow Column. Appl. Environ. Microbiol. 74, 5695–5703.
778 https://doi.org/10.1128/AEM.00926-08

779 Blazewicz, S.J., Barnard, R.L., Daly, R.A., Firestone, M.K., 2013. Evaluating rRNA as an
780 indicator of microbial activity in environmental communities: limitations and uses. ISME J.
781 7, 2061–2068. https://doi.org/10.1038/ismej.2013.102

782 Blázquez-Pallí, N., Rosell, M., Varias, J., Bosch, M., Soler, A., Vicent, T., Marco-Urrea, E.,
783 2019a. Multi-method assessment of the intrinsic biodegradation potential of an aquifer
784 contaminated with chlorinated ethenes at an industrial area in Barcelona (Spain). Environ.
785 Pollut. 244, 165–173. https://doi.org/10.1016/j.envpol.2018.10.013

786 Blázquez-Pallí, N., Rosell, M., Varias, J., Bosch, M., Soler, A., Vicent, T., Marco-Urrea, E.,
787 2019b. Integrative isotopic and molecular approach for the diagnosis and implementation
788 of an efficient in-situ enhanced biological reductive dechlorination of chlorinated ethenes.
789 Water Res. 167, 115106. https://doi.org/10.1016/j.watres.2019.115106

790 Blázquez-Pallí, N., Shouakar-Stash, O., Palau, J., Trueba-Santiso, A., Varias, J., Bosch, M.,
791 Soler, A., Vicent, T., Marco-Urrea, E., Rosell, M., 2019c. Use of dual element isotope
792 analysis and microcosm studies to determine the origin and potential anaerobic
793 biodegradation of dichloromethane in two multi-contaminated aquifers. Sci. Total Environ.
794 696, 134066. https://doi.org/10.1016/j.scitotenv.2019.134066

795 Bombach, P., Richnow, H.H., Kästner, M., Fischer, A., 2010. Current approaches for the
796 assessment of in situ biodegradation. Appl. Microbiol. Biotechnol. 86, 839–852.

https://doi.org/10.1007/s00253-010-2461-2

Bouwer, E.J., 1994. Bioremediation of chlorinated solvents using alternate electron acceptors, in: Norris, R.D. (Ed.), Handbook of Bioremediation. CRC Press, Boca Raton, pp. 149–176. https://doi.org/10.1201/9780203712764-9

Bradley, P.M., 2003. History and ecology of chloroethene biodegradation: a review. Bioremediat. J. 7, 81–109. https://doi.org/10.1080/713607980

Bradley, P.M., 2000. Microbial degradation of chloroethenes in groundwater systems. Hydrogeol. J. 8, 251–253. https://doi.org/10.1007/s100400050011

Brown, R.A., 2010. Chemical oxidation and reduction for chlorinated solvent remediation, in: Stroo, H.F., Ward, C.H. (Eds.), In Situ Remediation of Chlorinated Solvent Plumes. Springer US, New York, NY, pp. 481–535. https://doi.org/10.1007/978-1-4419-1401-9_15

Buchner, D., Behrens, S., Laskov, C., Haderlein, S.B., 2015. Resiliency of stable isotope fractionation (δ13C and δ37Cl) of trichloroethene to bacterial growth physiology and expression of key enzymes. Environ. Sci. Technol. 49, 13230–13237. https://doi.org/10.1021/acs.est.5b02918

Chen, G., Kara Murdoch, F., Xie, Y., Murdoch, R.W., Cui, Y., Yang, Y., Yan, J., Key, T.A., Löffler, F.E., 2022. Dehalogenation of Chlorinated Ethenes to Ethene by a Novel Isolate, “Candidatus Dehalogenimonas etheniformans.” Appl. Environ. Microbiol. 88. https://doi.org/10.1128/aem.00443-22

Coplen, T.B., 2011. Guidelines and recommended terms for expression of stable-isotope-ratio and gas-ratio measurement results. Rapid Commun. Mass Spectrom. 25, 2538–2560. https://doi.org/10.1002/rcm.5129

Coplen, T.B., 1996. New guidelines for reporting stable hydrogen, carbon, and oxygen isotope-ratio data. Geochim. Cosmochim. Acta 60, 3359–3360. https://doi.org/10.1016/0016-7037(96)00263-3

Cui, Y., Li, X., Yan, J., Lv, Y., Jin, H., Wang, J., Chen, G., Kara-Murdoch, F., Yang, Y., Löffler, F.E., 2023. Dehalogenimonas etheniformans sp. nov., a formate-oxidizing, organohalide-respiring bacterium isolated from grape pomace. Int. J. Syst. Evol. Microbiol. 73, 005881.

825 https://doi.org/10.1099/ijsem.0.005881

826 Cupples, A.M., 2008. Real-time PCR quantification of Dehalococcoides populations: Methods
827 and applications. J. Microbiol. Methods 72, 1–11.
828 https://doi.org/10.1016/j.mimet.2007.11.005

829 Custodio, E., Llamas, M.R., 1983. Hidrología Subterránea. Tomo I., 2nd Editio. ed. Ediciones
830 Omega, S.A., Barcelona.

831 Elsner, M., 2010. Stable isotope fractionation to investigate natural transformation mechanisms
832 of organic contaminants: principles, prospects and limitations. J. Environ. Monit. 12, 2005–
833 2031. https://doi.org/10.1039/c0em00277a

834 Elsner, M., Chartrand, M., VanStone, N., Lacrampe Couloume, G., Sherwood Lollar, B., 2008.
835 Identifying Abiotic Chlorinated Ethene Degradation: Characteristic Isotope Patterns in
836 Reaction Products with Nanoscale Zero-Valent Iron. Environ. Sci. Technol. 42, 5963–
837 5970. https://doi.org/10.1021/es8001986

838 Elsner, M., Hofstetter, T.B., 2011. Current Perspectives on the Mechanisms of
839 Chlorohydrocarbon Degradation in Subsurface Environments: Insight from Kinetics,
840 Product Formation, Probe Molecules, and Isotope Fractionation, in: Tratnyek, P.G.,
841 Grundl, T.J., Haderlein, S.B. (Eds.), Aquatic Redox Chemistry. American Chemical Society
842 (ACS Division of Environmental Chemistry and ACS Division of Geochemistry),
843 Washington, DC, pp. 407–439. https://doi.org/10.1021/bk-2011-1071.ch019

844 European Commission, 2022. EDO - European Drought Observatory [WWW Document].
845 Emerg. Manag. Serv. by Copernicus Program. URL https://joint-research-
846 centre.ec.europa.eu/european-and-global-drought-observatories/current-drought-situation-
847 europe_en (accessed 4.23.24).

848 European Commission, 2008. Directive 2008/105/EC of 16 December 2008 on environmental
849 quality standards in the field of water policy, Official Journal of the European Union.

850 European Commission, 2007. Mediterranean groundwater report - Technical report on
851 groundwater management in the Mediterranean and the water framework directive.
852 Publications Office of the European Union.

853 Fu, F., Dionysiou, D.D., Liu, H., 2014. The use of zero-valent iron for groundwater remediation
854 and wastewater treatment: A review. J. Hazard. Mater. 267, 194–205.
855 https://doi.org/10.1016/j.jhazmat.2013.12.062

856 Futagami, T., Furukawa, K., 2016. The genus Desulfitobacterium, in: L. Adrian and F.E. Löffler
857 (Ed) Organohalide-Respiring Bacteria. Springer Berlin Heidelberg, Berlin, Heidelberg, pp.
858 173–207. https://doi.org/10.1007/978-3-662-49875-0_9

859 Galdames, A., Ruiz-Rubio, L., Orueta, M., Sánchez-Arzalluz, M., Vilas-Vilela, J.L., 2020. Zero-
860 Valent Iron Nanoparticles for Soil and Groundwater Remediation. Int. J. Environ. Res.
861 Public Health 17, 5817. https://doi.org/10.3390/ijerph17165817

862 Guo, J., Gao, F., Zhang, C., Ahmad, S., Tang, J., 2023. Sulfidation of zero-valent iron for
863 enhanced reduction of chlorinated contaminants: A review on the reactivity, selectivity, and
864 interference resistance. Chem. Eng. J. 477, 147049.
865 https://doi.org/10.1016/j.cej.2023.147049

866 Hanert, H.H., 2006. The Genus Gallionella, in: The Prokaryotes. Springer New York, New York,
867 NY, pp. 990–995. https://doi.org/10.1007/0-387-30747-8_46

868 Herrero, J., Puigserver, D., Nijenhuis, I., Kuntze, K., Carmona, J.M., 2019. Combined use of
869 ISCR and biostimulation techniques in incomplete processes of reductive dehalogenation
870 of chlorinated solvents. Sci. Total Environ. 648, 819–829.
871 https://doi.org/10.1016/j.scitotenv.2018.08.184

872 Holliger, C., Regeard, C., Diekert, G., 2004. Dehalogenation by Anaerobic Bacteria, in:
873 Häggblom, M.M., Bossert, I.D. (Ed.), Dehalogenation. Springer US, Boston, MA, pp. 115–
874 157. https://doi.org/10.1007/0-306-48011-5_5

875 Hug, L.A., Edwards, E.A., 2013. Diversity of reductive dehalogenase genes from environmental
876 samples and enrichment cultures identified with degenerate primer PCR screens. Front.
877 Microbiol. 4, 16. https://doi.org/10.3389/fmicb.2013.00341

878 Hug, L.A., Maphosa, F., Leys, D., Löffler, F.E., Smidt, H., Edwards, E.A., Adrian, L., 2013.
879 Overview of organohalide-respiring bacteria and a proposal for a classification system for
880 reductive dehalogenases. Philos. Trans. R. Soc. B Biol. Sci. 368, 10.

881 https://doi.org/10.1098/rstb.2012.0322

882 Hunkeler, D., Aravena, R., Butler, B.J., 1999. Monitoring microbial dechlorination of
883 tetrachloroethene (PCE) in groundwater using compound-specific stable carbon isotope
884 ratios: Microcosm and field studies. Environ. Sci. Technol. 33, 2733–2738.
885 https://doi.org/10.1021/es981282u

886 Hunkeler, D., Meckenstock, R.U., Lollar, B.S., Schmidt, T.C., Wilson, J.T., 2008. A guide for
887 assessing biodegradation and source identification of organic ground water contaminants
888 using compound specific isotope analysis (CSIA), U.S. Environmental Protection Agency.
889 Washington, D.C., EPA/600/R-08/148.

890 Imfeld, G., Nijenhuis, I., Nikolausz, M., Zeiger, S., Paschke, H., Drangmeister, J., Grossmann,
891 J., Richnow, H.H., Weber, S., 2008. Assessment of in situ degradation of chlorinated
892 ethenes and bacterial community structure in a complex contaminated groundwater
893 system. Water Res. 42, 871–882. https://doi.org/10.1016/j.watres.2007.08.035

894 Kocur, C.M.D., Lomheim, L., Molenda, O., Weber, K.P., Austrins, L.M., Sleep, B.E., Boparai,
895 H.K., Edwards, E.A., O'Carroll, D.M., 2016. Long-Term Field Study of Microbial
896 Community and Dechlorinating Activity Following Carboxymethyl Cellulose-Stabilized
897 Nanoscale Zero-Valent Iron Injection. Environ. Sci. Technol. 50, 7658–7670.
898 https://doi.org/10.1021/acs.est.6b01745

899 Krajmalnik-Brown, R., Hölscher, T., Thomson, I.N., Saunders, F.M., Ritalahti, K.M., Löffler, F.E.,
900 2004. Genetic identification of a putative vinyl chloride reductase in Dehalococcoides sp.
901 strain BAV1. Appl. Environ. Microbiol. 70, 6347–6351.
902 https://doi.org/10.1128/AEM.70.10.6347-6351.2004

903 Krzmarzick, M.J., Crary, B.B., Harding, J.J., Oyerinde, O.O., Leri, A.C., Myneni, S.C.B., Novak,
904 P.J., 2012. Natural Niche for Organohalide-Respiring Chloroflexi. Appl. Environ. Microbiol.
905 78, 393–401. https://doi.org/10.1128/AEM.06510-11

906 Kuntze, K., Eisenmann, H., Richnow, H.-H., Fischer, A., 2019. Compound-Specific Stable
907 Isotope Analysis (CSIA) for Evaluating Degradation of Organic Pollutants: An Overview of
908 Field Case Studies, in: Anaerobic Utilization of Hydrocarbons, Oils, and Lipids. Springer
909 International Publishing, Cham, pp. 1–39. https://doi.org/10.1007/978-3-319-33598-8_23-1

910 Lee, J., Im, J., Kim, U., Löffler, F.E., 2016. A data mining approach to predict in situ
911 detoxification potential of chlorinated ethenes. Environ. Sci. Technol. 50, 5181–5188.
912 https://doi.org/10.1021/acs.est.5b05090

913 Leeson, A., Beevar, E., Henry, B.M., Fortenberry, J., Coyle, C., Parsons Corp., 2004. Principles
914 and practices of enhanced anaerobic bioremediation of chlorinated solvents. Port
915 Hueneme, California, ESTCP CU 0125.

916 Löffler, F.E., Cole, J.R., Ritalahti, K.M., Tiedje, J.M., 2004. Diversity of Dechlorinating Bacteria,
917 in: Häggblom, M.M., Bossert, I.D. (Eds.), Dehalogenation. Springer US, Boston, MA, pp.
918 53–87. https://doi.org/10.1007/0-306-48011-5_3

919 Löffler, F.E., Ritalahti, K.M., Zinder, S.H., 2013a. Dehalococcoides and reductive dechlorination
920 of chlorinated solvents, in: Stroo, H.F., Leeson, A., Ward, C.H. (Eds.), Bioaugmentation for
921 Groundwater Remediation. Springer, New York, NY, pp. 39–88.
922 https://doi.org/10.1007/978-1-4614-4115-1_2

923 Löffler, F.E., Yan, J., Ritalahti, K.M., Adrian, L., Edwards, E.A., Konstantinidis, K.T., Müller, J.A.,
924 Fullerton, H., Zinder, S.H., Spormann, A.M., 2013b. Dehalococcoides mccartyi gen. nov.,
925 sp. nov., obligately organohalide-respiring anaerobic bacteria relevant to halogen cycling
926 and bioremediation, belong to a novel bacterial class, Dehalococcoidia classis nov., order
927 Dehalococcoidales ord. nov. and famil. Int. J. Syst. Evol. Microbiol. 63, 625–635.
928 https://doi.org/10.1099/ijs.0.034926-0

929 Loganathan, B.G., Lam, P.K.S., 2011. Global contamination trends of persistent organic
930 chemicals, 1st ed. CRC Press, Boca Raton.

931 Madison, A.S., Sorsby, S.J., Wang, Y., Key, T.A., 2023. Increasing in situ bioremediation
932 effectiveness through field-scale application of molecular biological tools. Front. Microbiol.
933 13, 1005871. https://doi.org/10.3389/fmicb.2022.1005871

934 Martín-González, L., Mortan, S.H., Rosell, M., Parladé, E., Martínez-Alonso, M., Gaju, N.,
935 Caminal, G., Adrian, L., Marco-Urrea, E., 2015. Stable carbon isotope fractionation during
936 1,2-dichloropropane-to-propene transformation by an enrichment culture containing
937 Dehalogenimonas strains and a dcpA gene. Environ. Sci. Technol. 49, 8666–74.
938 https://doi.org/10.1021/acs.est.5b00929

939 Mattes, T.E., Alexander, A.K., Coleman, N. V., 2010. Aerobic biodegradation of the
940 chloroethenes: Pathways, enzymes, ecology, and evolution. FEMS Microbiol. Rev. 34,
941 445–475. https://doi.org/10.1111/j.1574-6976.2010.00210.x

942 Matteucci, F., Ercole, C., Del Gallo, M., 2015. A study of chlorinated solvent contamination of
943 the aquifers of an industrial area in central Italy: A possibility of bioremediation. Front.
944 Microbiol. 6, 1–10. https://doi.org/10.3389/fmicb.2015.00924

945 McCarty, P.L., Semprini, L., 1994. Ground-water treatment for chlorinated solvents, in: Norris
946 RD, Hinchee RE, Brown R, McCarty PL, Semprini L, Wilson DH, Kampbell M, Reinhard
947 EG, Bouwer R, Borden C, Vogel TM, Thomas JM, W.C. (Ed.), Handbook of
948 Bioremediation. CRC Press, pp. 87–116.

949 McInerney, M.J., Bryant, M.P., Hespell, R.B., Costerton, J.W., 1981. Syntrophomonas wolfei
950 gen. nov. sp. nov., an Anaerobic, Syntrophic, Fatty Acid-Oxidizing Bacterium. Appl.
951 Environ. Microbiol. 41, 1029–1039. https://doi.org/10.1128/aem.41.4.1029-1039.1981

952 McKelvie, J.R., Hirschorn, S.K., Lacrampe-Couloume, G., Lindstrom, J., Braddock, J., Finneran,
953 K., Trego, D., Lollar, B.S., 2007. Evaluation of TCE and MTBE in situ Biodegradation:
954 Integrating Stable Isotope, Metabolic Intermediate, and Microbial Lines of Evidence.
955 Groundw. Monit. Remediat. 27, 63–73. https://doi.org/10.1111/j.1745-6592.2007.00170.x

956 Moran, M.J., 2006. Occurrence and implications of selected chlorinated solvents in groundwater
957 and source water in the United States and in drinking water in 12 northeast and mid-
958 atlantic states, 1993–2002, Scientific Investigations Report 2005–5268. Reston, Virginia.

959 Moran, M.J., Zogorski, J.S., Squillace, P.J., 2007. Chlorinated solvents in groundwater of the
960 United States. Environ. Sci. Technol. 41, 74–81. https://doi.org/10.1021/es061553y

961 Muller, J.A., Rosner, B.M., von Abendroth, G., Meshulam-Simon, G., McCarty, P.L., Spormann,
962 A.M., 2004. Molecular identification of the catabolic vinyl chloride reductase from
963 Dehalococcoides sp. strain VS and its environmental distribution. Appl. Environ. Microbiol.
964 70, 4880–4888. https://doi.org/10.1128/AEM.70.8.4880-4888.2004

965 National Research Council, 1999. Groundwater & soil cleanup: improving management of
966 persistent contaminants. National Academies Press.

967 Nijenhuis, I., Kuntze, K., 2016. Anaerobic microbial dehalogenation of organohalides-state of
968 the art and remediation strategies. Curr. Opin. Biotechnol. 38, 33–38.
969 https://doi.org/10.1016/j.copbio.2015.11.009

970 Nijenhuis, I., Nikolausz, M., Köth, A., Felföldi, T., Weiss, H., Drangmeister, J., Großmann, J.,
971 Kästner, M., Richnow, H.H., 2007. Assessment of the natural attenuation of chlorinated
972 ethenes in an anaerobic contaminated aquifer in the Bitterfeld/Wolfen area using stable
973 isotope techniques, microcosm studies and molecular biomarkers. Chemosphere 67, 300–
974 311. https://doi.org/10.1016/j.chemosphere.2006.09.084

975 Nijenhuis, I., Richnow, H.H., 2016. Stable isotope fractionation concepts for characterizing
976 biotransformation of organohalides. Curr. Opin. Biotechnol. 41, 108–113.
977 https://doi.org/10.1016/j.copbio.2016.06.002

978 Nunez Garcia, A., Boparai, H.K., Chowdhury, A.I.A., de Boer, C. V., Kocur, C.M.D., Passeport,
979 E., Sherwood Lollar, B., Austrins, L.M., Herrera, J., O'Carroll, D.M., 2020. Sulfidated nano
980 zerovalent iron (S-nZVI) for in situ treatment of chlorinated solvents: A field study. Water
981 Res. 174, 115594. https://doi.org/10.1016/j.watres.2020.115594

982 Ojeda, A.S., Phillips, E., Sherwood Lollar, B., 2020. Multi-element (C, H, Cl, Br) stable isotope
983 fractionation as a tool to investigate transformation processes for halogenated
984 hydrocarbons. Environ. Sci. Process. Impacts 22, 567–582.
985 https://doi.org/10.1039/C9EM00498J

986 Ottosen, C.B., Bjerg, P.L., Hunkeler, D., Zimmermann, J., Tuxen, N., Harrekilde, D.,
987 Bennedsen, L., Leonard, G., Brabæk, L., Kristensen, I.L., Broholm, M.M., 2021.
988 Assessment of chlorinated ethenes degradation after field scale injection of activated
989 carbon and bioamendments: Application of isotopic and microbial analyses. J. Contam.
990 Hydrol. 240, 103794. https://doi.org/10.1016/j.jconhyd.2021.103794

991 Palau, J., Marchesi, M., Chambon, J.C.C., Aravena, R., Canals, À., Binning, P.J., Bjerg, P.L.,
992 Otero, N., Soler, A., 2014. Multi-isotope (carbon and chlorine) analysis for fingerprinting
993 and site characterization at a fractured bedrock aquifer contaminated by chlorinated
994 ethenes. Sci. Total Environ. 475, 61–70. https://doi.org/10.1016/j.scitotenv.2013.12.059

995 Panagos, P., Van Liedekerke, M., Yigini, Y., Montanarella, L., 2013. Contaminated sites in

996 Europe: Review of the current situation based on data collected through a European
997 Network. J. Environ. Public Health 2013, 1–11. https://doi.org/10.1155/2013/158764

998 Philips, J., Haest, P.J., Springael, D., Smolders, E., 2013. Inhibition of Geobacter Dechlorinators
999 at Elevated Trichloroethene Concentrations Is Explained by a Reduced Activity Rather
1000 than by an Enhanced Cell Decay. Environ. Sci. Technol. 47, 130115145641003.
1001 https://doi.org/10.1021/es303390q

1002 Prommer, H., Aziz, L.H., Bolaño, N., Taubald, H., Schüth, C., 2008. Modelling of geochemical
1003 and isotopic changes in a column experiment for degradation of TCE by zero-valent iron.
1004 J. Contam. Hydrol. 97, 13–26. https://doi.org/10.1016/j.jconhyd.2007.11.003

1005 Renpenning, J., Nijenhuis, I., 2016. Evaluation of the Microbial Reductive Dehalogenation
1006 Reaction Using Compound-Specific Stable Isotope Analysis (CSIA), in: Adrian, L., Löffler,
1007 F.E. (Eds.), Organohalide-Respiring Bacteria. Springer Berlin Heidelberg, Berlin,
1008 Heidelberg, pp. 429–453. https://doi.org/10.1007/978-3-662-49875-0_18

1009 Salom, D., Fernández-Verdejo, D., Moral-Vico, J., Font, X., Marco-Urrea, E., 2023. Combining
1010 nanoscale zero-valent iron and anaerobic dechlorinating bacteria to degrade chlorinated
1011 methanes and 1,2-dichloroethane. Environ. Sci. Pollut. Res. 1, 1–13.
1012 https://doi.org/10.1007/s11356-023-25376-z

1013 Sheu, Y.T., Lien, P.J., Chen, K.F., Ou, J.H., Kao, C.M., 2016. Application of NZVI-contained
1014 emulsified substrate to bioremediate PCE-contaminated groundwater – A pilot-scale study.
1015 Chem. Eng. J. 304, 714–727. https://doi.org/10.1016/j.cej.2016.06.126

1016 Şimşir, B., Yan, J., Im, J., Graves, D., Löffler, F.E., 2017. Natural Attenuation in Streambed
1017 Sediment Receiving Chlorinated Solvents from Underlying Fracture Networks. Environ.
1018 Sci. Technol. 51, 4821–4830. https://doi.org/10.1021/acs.est.6b05554

1019 Smidt, H., de Vos, W.M., 2004. Anaerobic Microbial Dehalogenation. Annu. Rev. Microbiol. 58,
1020 43–73. https://doi.org/10.1146/annurev.micro.58.030603.123600

1021 Stroo, H.F., Ward, C.H., 2010. In situ remediation of chlorinated solvent plumes, 1st ed,
1022 SERDP/ESTCP Environmental Remediation Technology. Springer New York, New York,
1023 NY. https://doi.org/10.1007/978-1-4419-1401-9

1024 Tarnawski, S.-E., Rossi, P., Brennerova, M. V., Stavelova, M., Holliger, C., 2016. Validation of
1025 an Integrative Methodology to Assess and Monitor Reductive Dechlorination of
1026 Chlorinated Ethenes in Contaminated Aquifers. Front. Environ. Sci. 4, 1–16.
1027 https://doi.org/10.3389/fenvs.2016.00007

1028 Trueba-Santiso, A., Palau, J., Soder-Walz, J.M., Vicent, T., Marco-Urrea, E., 2022. Assessment
1029 of aerobic biodegradation of lower-chlorinated benzenes in contaminated groundwater
1030 using field-derived microcosms and compound-specific carbon isotope fractionation. J.
1031 Environ. Sci. https://doi.org/10.1016/j.jes.2021.12.025

1032 Tukanghan, W., Hupfauf, S., Gómez-Brandón, M., Insam, H., Salvenmoser, W., Prasertsan, P.,
1033 Cheirsilp, B., O-Thong, S., 2021. Symbiotic Bacteroides and Clostridium-rich
1034 methanogenic consortium enhanced biogas production of high-solid anaerobic digestion
1035 systems. Bioresour. Technol. Reports 14, 100685.
1036 https://doi.org/10.1016/j.biteb.2021.100685

1037 US EPA, 2014. Toxic and Priority Pollutants Under the Clean Water Act, 40 CFR Part 423,
1038 Appendix A.

1039 van der Zaan, B., Hannes, F., Hoekstra, N., Rijnaarts, H., de Vos, W.M., Smidt, H., Gerritse, J.,
1040 2010. Correlation of Dehalococcoides 16S rRNA and Chloroethene-Reductive
1041 Dehalogenase Genes with Geochemical Conditions in Chloroethene-Contaminated
1042 Groundwater. Appl. Environ. Microbiol. 76, 843–850. https://doi.org/10.1128/AEM.01482-
1043 09

1044 VanStone, N.A., Focht, R.M., Mabury, S.A., Lollar, B.S., 2004. Effect of Iron Type on Kinetics
1045 and Carbon Isotopic Enrichment of Chlorinated Ethylenes During Abiotic Reduction on
1046 Fe(0). Groundwater 42, 268–276. https://doi.org/10.1111/j.1745-6584.2004.tb02673.x

1047 Vogel, T.M., 1994. Natural bioremediation of chlorinated solvents, in: Norris RD, Hinchee RE,
1048 Brown R, McCarty PL, Semprini L, Wilson DH, Kampbell M, Reinhard EG, Bouwer R,
1049 Borden C, Vogel TM, Thomas JM, W.C. (Ed.), Handbook of Bioremediation. CRC Press,
1050 pp. 201–225.

1051 Vogel, T.M., Criddle, C.S., McCarty, P.L., 1987. ES&T Critical Review: Transformations of
1052 halogenated aliphatic compounds. Environ. Sci. Technol. 21, 722–736.

https://doi.org/10.1021/es00162a001

Wang, S., Chen, S., Wang, Y., Low, A., Lu, Q., Qiu, R., 2016. Integration of organohalide-respiring bacteria and nanoscale zero-valent iron (Bio-nZVI-RD): A perfect marriage for the remediation of organohalide pollutants? Biotechnol. Adv. 34, 1384–1395. https://doi.org/10.1016/j.biotechadv.2016.10.004

Werner, R.A., Brand, W.A., 2001. Referencing strategies and techniques in stable isotope ratio analysis. Rapid Commun. Mass Spectrom. 15, 501–519. https://doi.org/10.1002/rcm.258

Wiedemeier, T.H., Swanson, M.A., Moutoux, D.E., Gordon, E.K., Wilson, J.T., Wilson, B.H., Kampbell, D.H., Haas, P.E., Miller, R.N., Hansen, J.E., Chapelle., F. H., Kinzie Gordon, E., Wilson, J.T., Wilson, B.H., Kampbell, D.H., Haas, P.E., Miller, R.N., Hansen, J.E., Chapelle, Francis H, 1998. Technical protocol for evaluating natural attenuation of chlorinated solvents in ground water, U.S. Environmental Protection Agency, EPA/600/R-98/128 (NTIS 99-130023). U.S. EPA, Washington DC 20460.

Willems, A., 2014. The Family Comamonadaceae, in: The Prokaryotes. Springer Berlin Heidelberg, Berlin, Heidelberg, pp. 777–851. https://doi.org/10.1007/978-3-642-30197-1_238

Wu, N., Zhang, W., Wei, W., Yang, S., Wang, H., Sun, Z., Song, Y., Li, P., Yang, Y., 2020. Field study of chlorinated aliphatic hydrocarbon degradation in contaminated groundwater via micron zero-valent iron coupled with biostimulation. Chem. Eng. J. 384, 123349. https://doi.org/10.1016/j.cej.2019.123349

Yan, J., Rash, B.A., Rainey, F.A., Moe, W.M., 2009. Detection and Quantification of Dehalogenimonas and “Dehalococcoides” Populations via PCR-Based Protocols Targeting 16S rRNA Genes. Appl. Environ. Microbiol. 75, 7560–7564. https://doi.org/10.1128/AEM.01938-09

Yan, J., Wang, J., Villalobos Solis, M.I., Jin, H., Chourey, K., Li, X., Yang, Y., Yin, Y., Hettich, R.L., Löffler, F.E., 2021. Respiratory Vinyl Chloride Reductive Dechlorination to Ethene in TceA-Expressing Dehalococcoides mccartyi. Environ. Sci. Technol. 55, 4831–4841. https://doi.org/10.1021/acs.est.0c07354

1081 Yang, J., Meng, L., Guo, L., 2018. In situ remediation of chlorinated solvent-contaminated
1082 groundwater using ZVI/organic carbon amendment in China: field pilot test and full-scale
1083 application. Environ. Sci. Pollut. Res. 25, 5051–5062. https://doi.org/10.1007/s11356-017-
1084 9903-7

1085 Yang, Y., Cápiro, N.L., Marcet, T.F., Yan, J., Pennell, K.D., Löffler, F.E., 2017a. Organohalide
1086 respiration with chlorinated ethenes under low pH conditions. Environ. Sci. Technol. 51,
1087 8579–8588. https://doi.org/10.1021/acs.est.7b01510

1088 Yang, Y., Higgins, S.A., Yan, J., Şimşir, B., Chourey, K., Iyer, R., Hettich, R.L., Baldwin, B.R.,
1089 Ogles, D.M., Löffler, F.E., 2017b. Grape pomace compost harbors organohalide-respiring
1090 Dehalogenimonas species with novel reductive dehalogenase genes. ISME J. 11, 2767–
1091 2780. https://doi.org/10.1038/ismej.2017.127

1092 Yi, M., Zhang, L., Qin, C., Lu, P., Bai, H., Han, X., Yuan, S., 2022. Temporal changes of
1093 microbial community structure and nitrogen cycling processes during the aerobic
1094 degradation of phenanthrene. Chemosphere 286, 131709.
1095 https://doi.org/10.1016/j.chemosphere.2021.131709

1096 Yu, R., Andrachek, R.G., Lehmicke, L.G., Freedman, D.L., 2018. Remediation of chlorinated
1097 ethenes in fractured sandstone by natural and enhanced biotic and abiotic processes: A
1098 crushed rock microcosm study. Sci. Total Environ. 626, 497–506.
1099 https://doi.org/10.1016/j.scitotenv.2018.01.064

1100 Zinder, S.H., 2016. The genus Dehalococcoides, in: L. Adrian and F.E. Löffler (Ed)
1101 Organohalide-Respiring Bacteria. Springer Berlin Heidelberg, Berlin, Heidelberg, pp. 107–
1102 136. https://doi.org/10.1007/978-3-662-49875-0_6

1103 Zogorski, J.S., Carter, J.M., Ivahnenko, T., Lapham, W.W., Moran, M.J., Rowe, B.L., Squillace,
1104 P.J., Toccalino, P.L., 2006. The quality of our nation's waters: Volatile organic compounds
1105 in the nation's groundwater and drinking-water supply wells, U.S. Geological Survey
1106 Circular 1292. Reston, Virginia.

1107

Table (Editable version) Click here to access/download;Table (Editable version);renamed_f19be.docx

Table 1. Nomenclature table, listing all used abbreviations and symbols and their definitions.

Abbreviated notation	Description
^{12}C	Carbon-12 isotope
^{13}C	Carbon-13 isotope
16S rRNA	16S ribosomal ribonucleic acid
B-ISCR	Combined bioremediation and in situ chemical reduction
BvcA	Vinyl chloride reductive dehalogenase
CEs	Chlorinated ethenes
CI	Confidence interval
cis-DCE	cis-1,2-dichloroethylene
CSIA	Compound-specific stable isotope analysis
%D	Biodegradation efficiency or extent of degradation
Dhc	*Dehalococcoides*
Dhg	*Dehalogenimonas*
DNA	Deoxyribonucleic acid
DNAPL	Dense non-aqueous phase liquid
DO	Dissolved oxygen
EC	Electrical conductivity
Eh	Corrected redox potential (corrected ORP)
ETH	Ethylene or ethene
FID	Flame ionization detector
GC	Gas chromatography
GC-IRMS	Gas chromatography-isotope ratio mass spectrometry
GC-MS	Gas chromatography-mass spectrometry
HS-SPME	Headspace solid-phase microextraction
ICP-MS	Inductively coupled plasma mass spectrometry
ISCR	In situ chemical reduction
LOQ	Limit of quantification
mZVI	Microscale zero-valent iron
N.E.W.	North exploitation well
nZVI	Nanoscale zero-valent iron
OHRB	Organohalide-respiring bacteria
ORP	Oxidation-reduction potential (measured in situ)
OTU	Operational taxonomic unit
PCE	Tetrachloroethylene or perchloroethylene
PceA	Tetrachloroethylene reductive dehalogenase
PCR	Polymerase chain reaction
qPCR	Quantitative polymerase chain reaction
S.E.W.	South exploitation well
SHE	Standard hydrogen electrode
SI	Supporting information
T	Temperature
T0	Time zero (prior to the start of the pilot tests)
TCE	Trichloroethylene
TceA	Trichloroethylene reductive dehalogenase
TF	Time final (after or at the conclusion of the pilot tests)
VC	Vinyl chloride
VcrA	Vinyl chloride reductive dehalogenase

Abbreviated notation	Description
VPDB	Vienna Pee Dee Belemnite
ZVI	Zero-valent iron
δ	Isotope composition (delta notation)
$\delta^{13}C$	Delta carbon-13 (carbon isotopic composition)
$\delta^{13}C_n$	Carbon isotopic composition for a specific compound (n)
$\delta^{13}C_{SUM}$	Carbon isotopic mass balance
$\Delta\delta^{13}C$	Shifts in carbon isotope composition
ε	Isotope fractionation
εC	Carbon isotope fractionation
εC_n	εC for a specific compound (n)

Figure 1

Click here to access/download;Figure;Figure 1.jpg

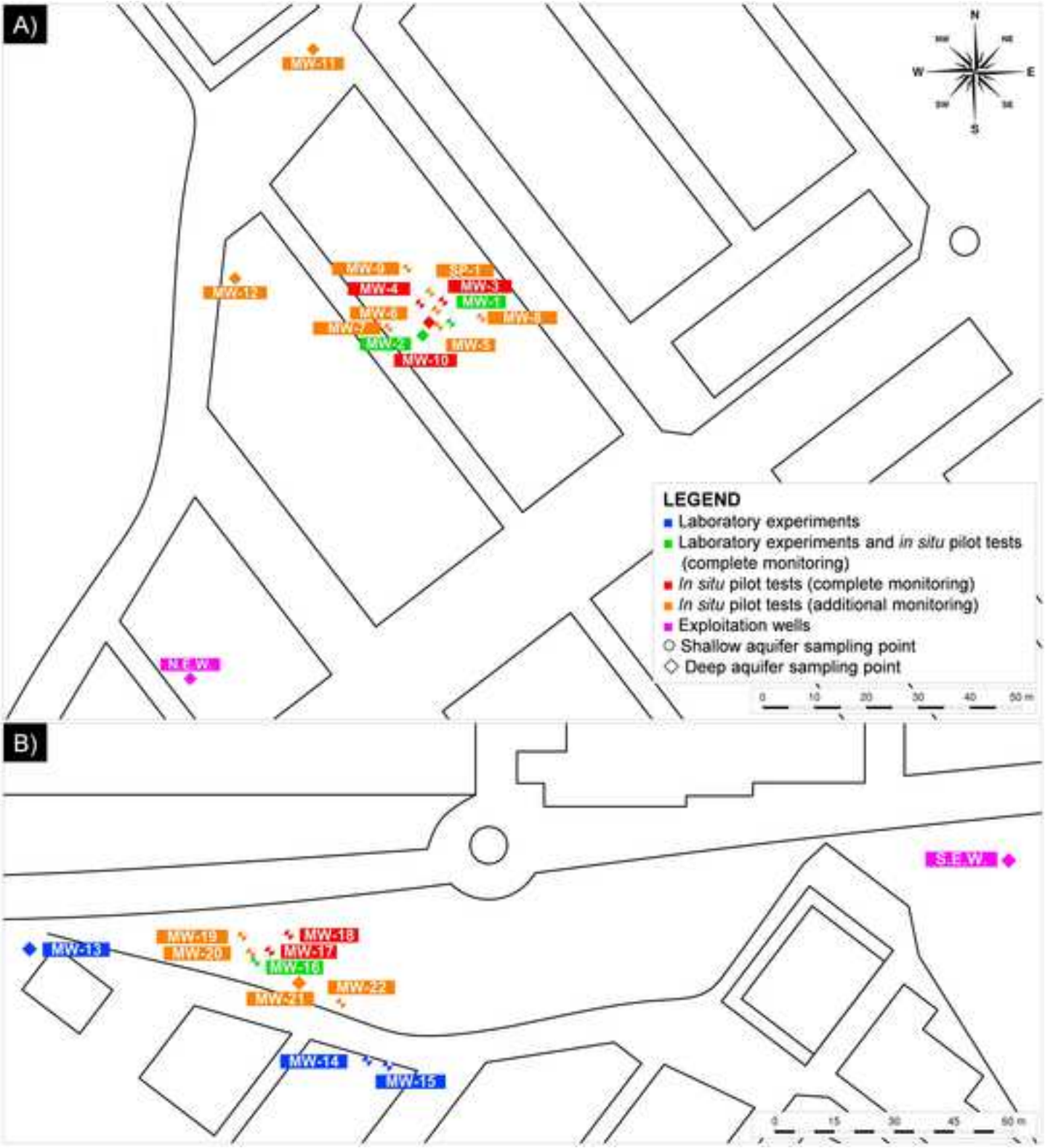


Figure 2

Click here to access/download;Figure;Figure 2.jpg

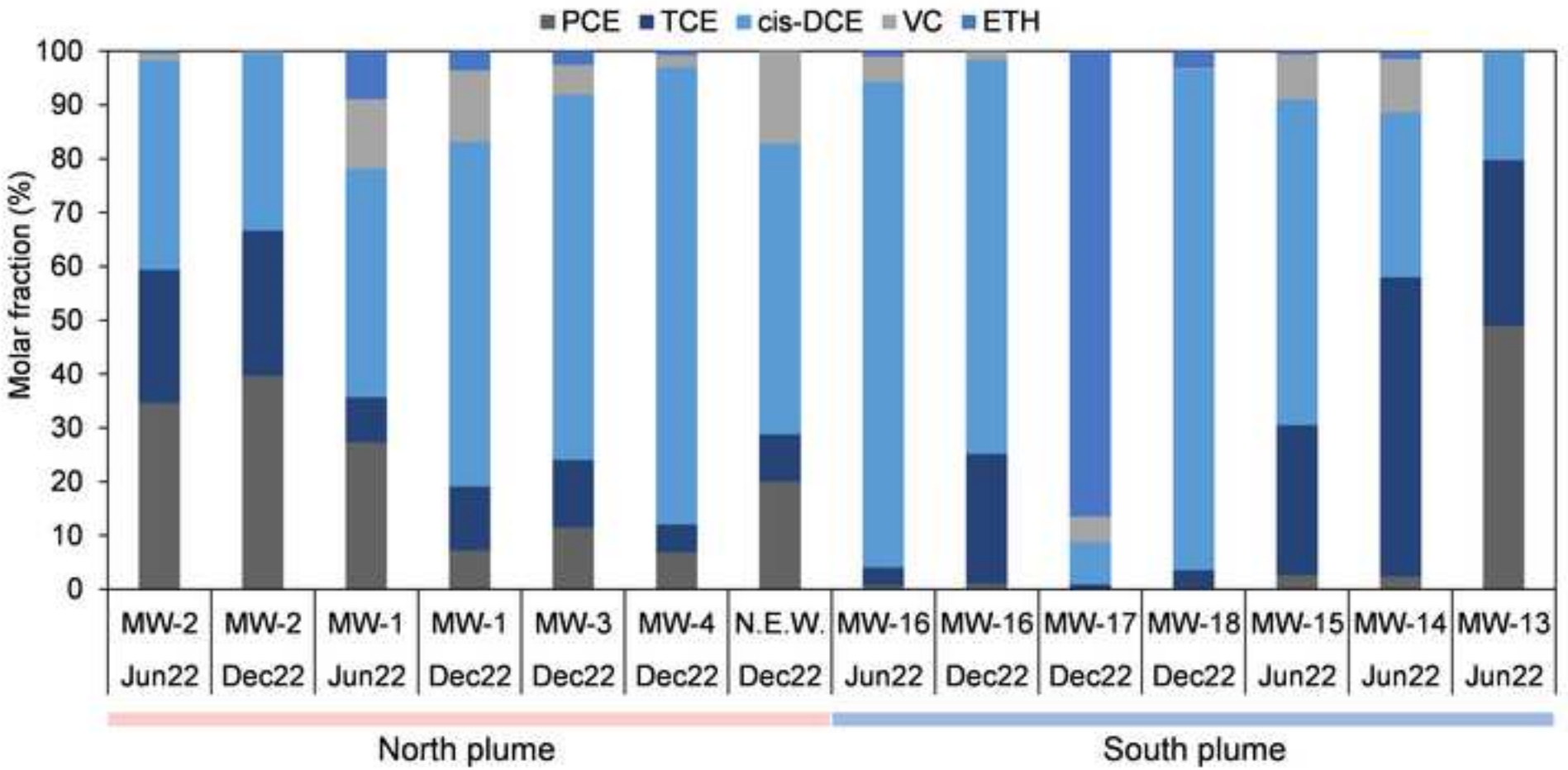


Figure 3

Click here to access/download;Figure;Figure 3.jpg

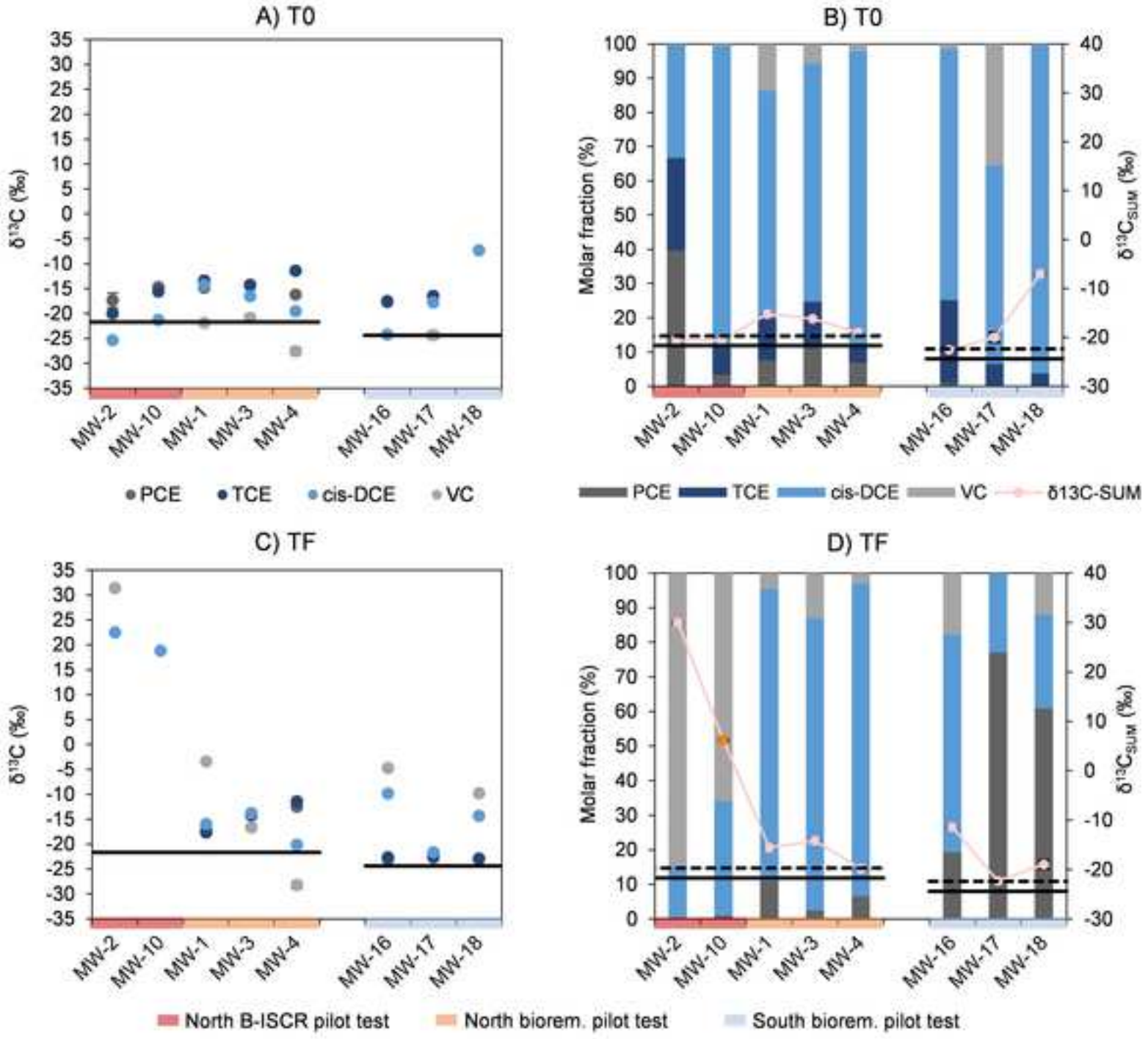


Figure 4

Click here to access/download;Figure;Figure 4.jpg

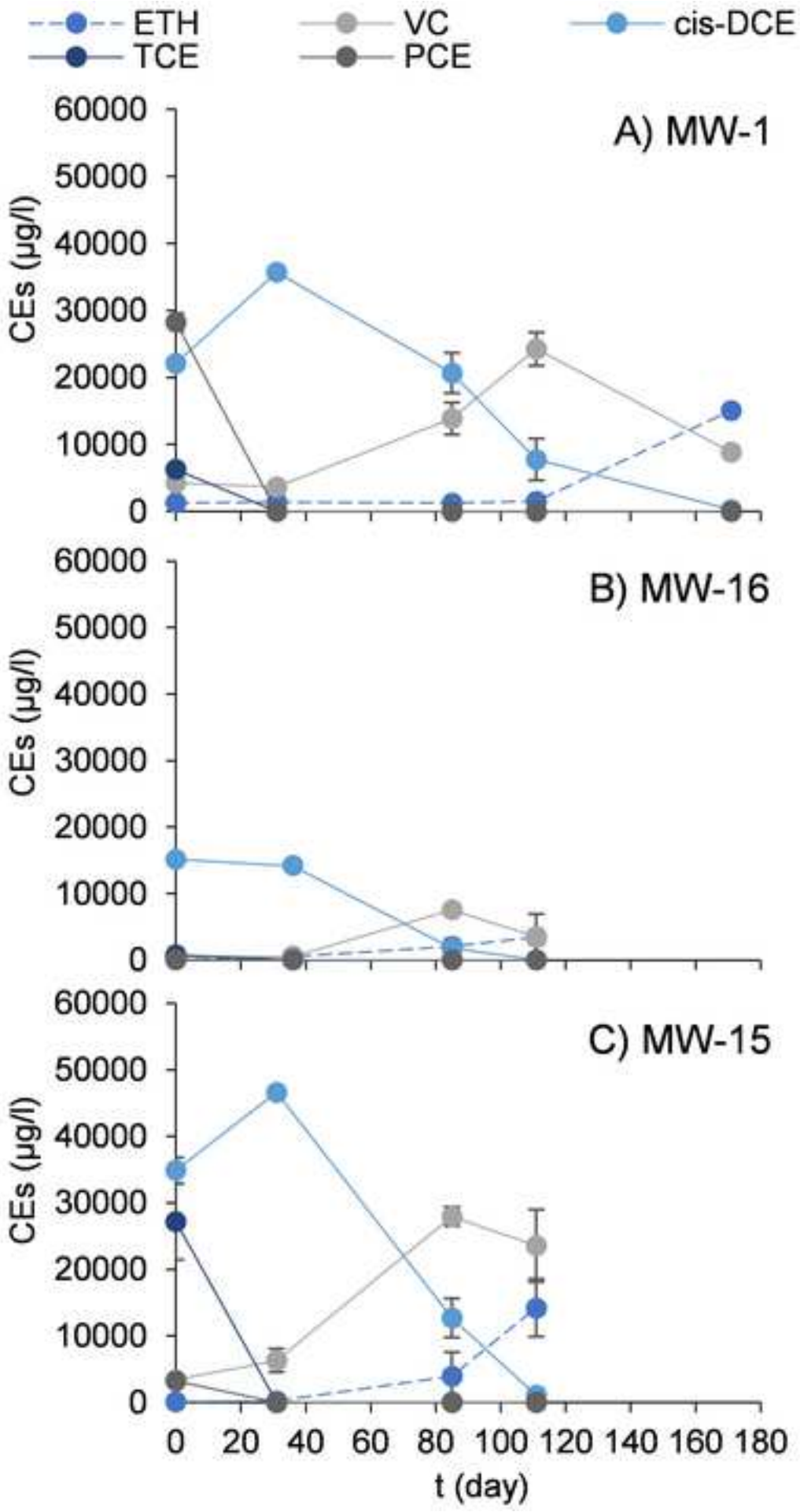


Figure 5

Click here to access/download;Figure;Figure 5.jpg

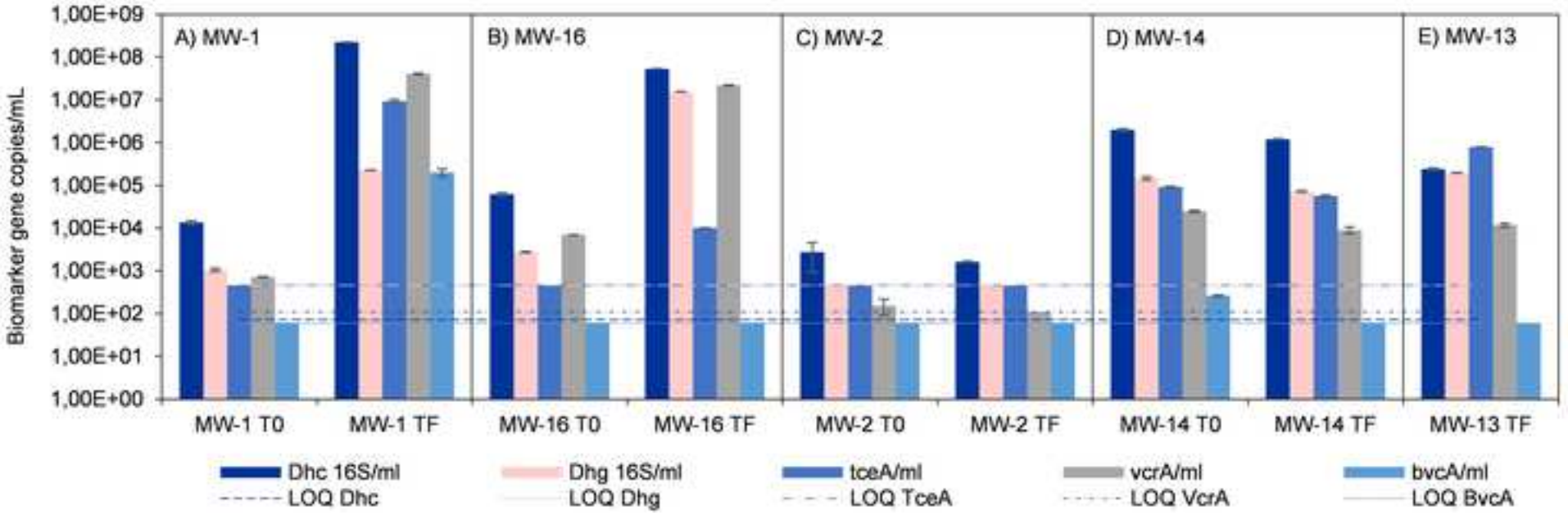


Figure 6

Click here to access/download;Figure;Figure 6.jpg

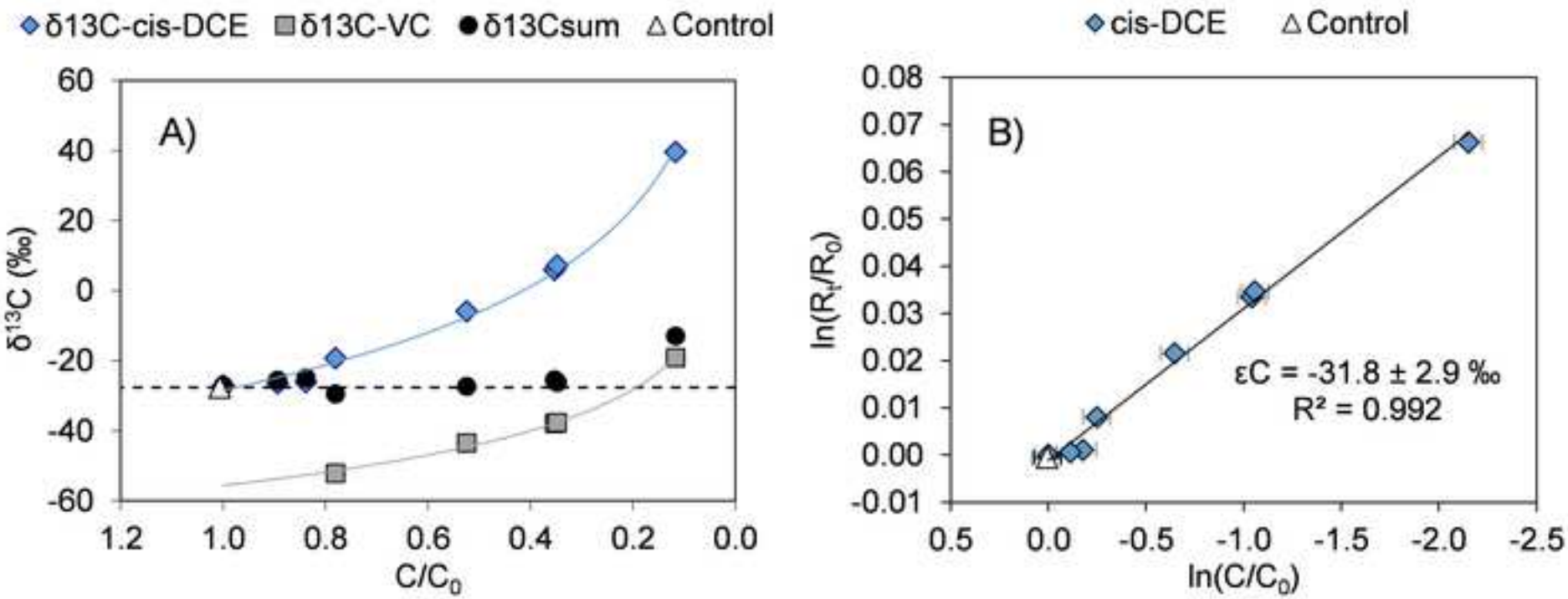


Figure 7

Click here to access/download;Figure;Figure 7.jpg

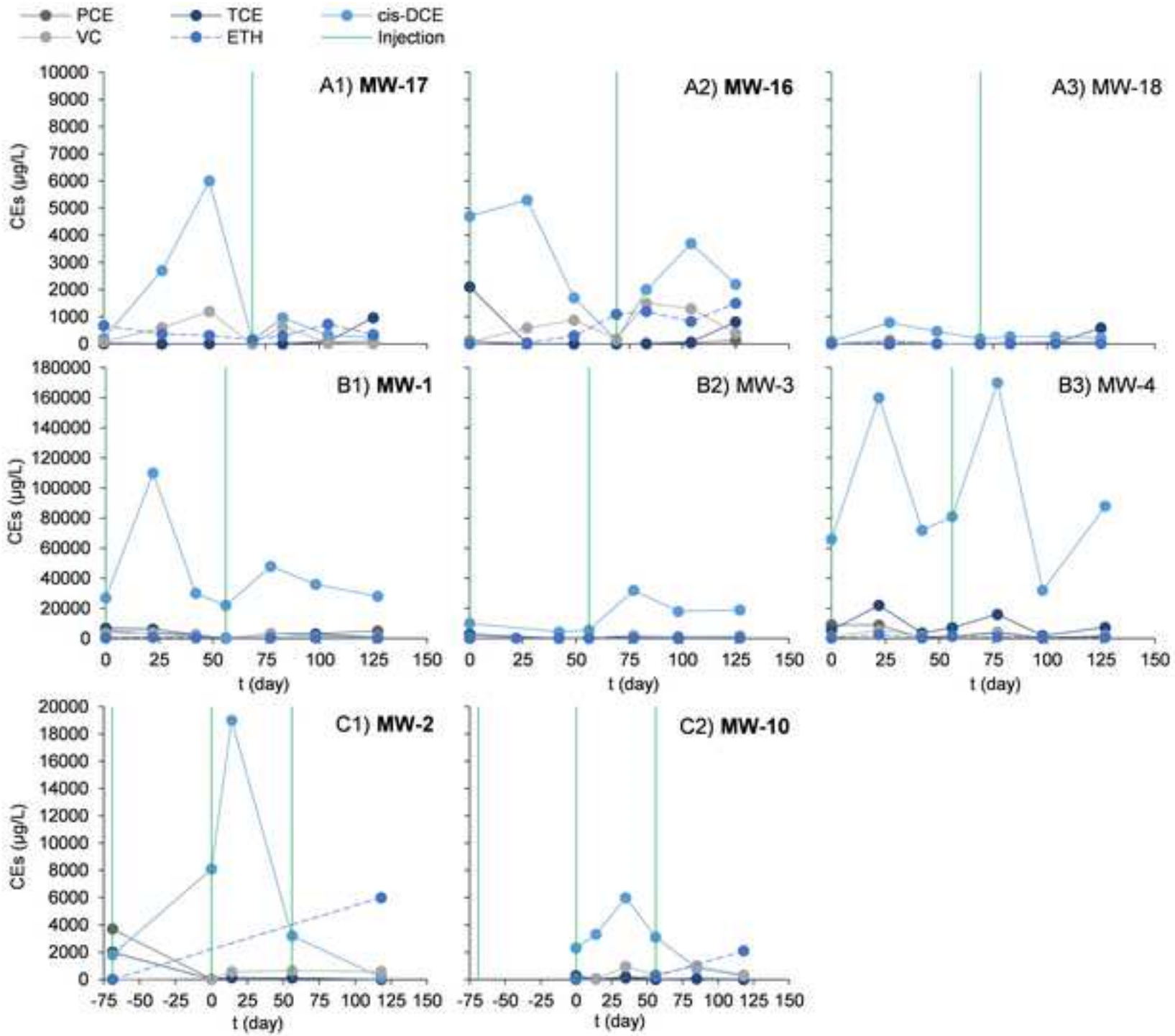
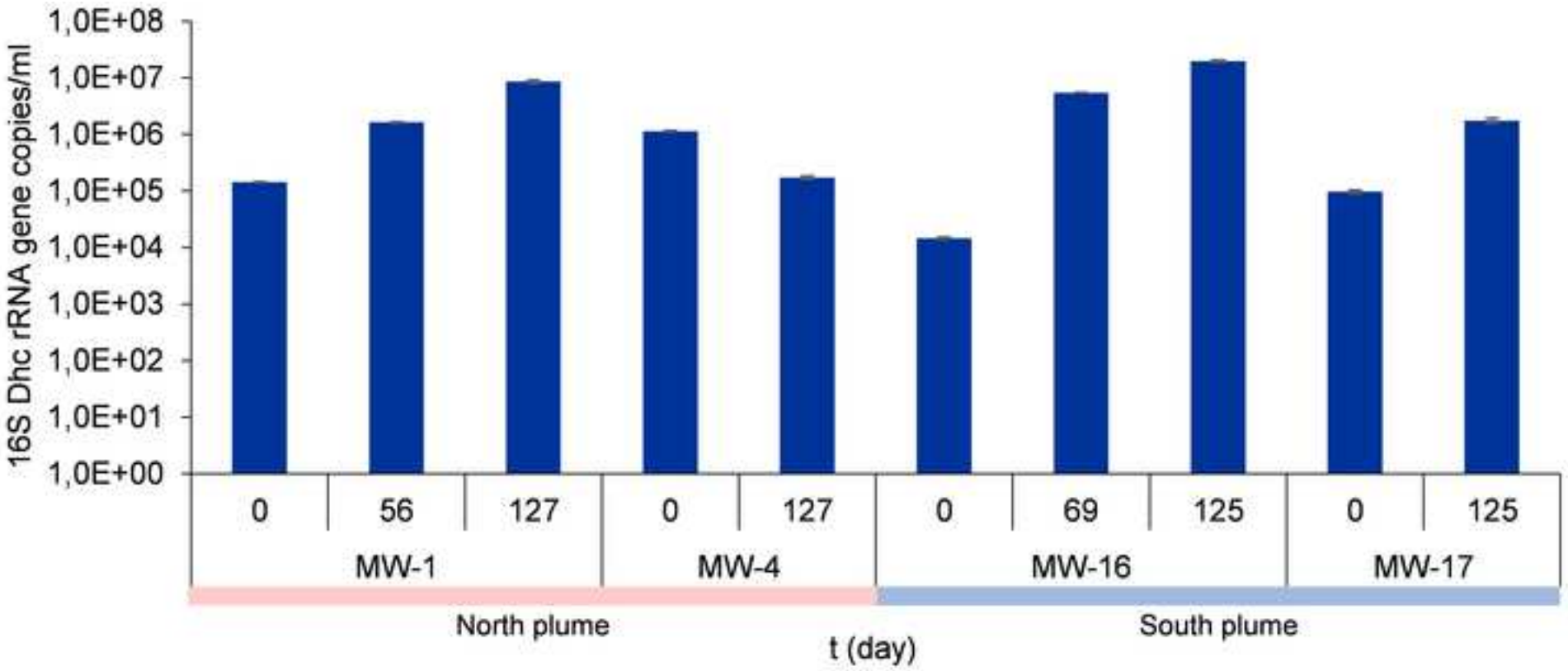


Figure 8

Click here to access/download;Figure;Figure 8.jpg



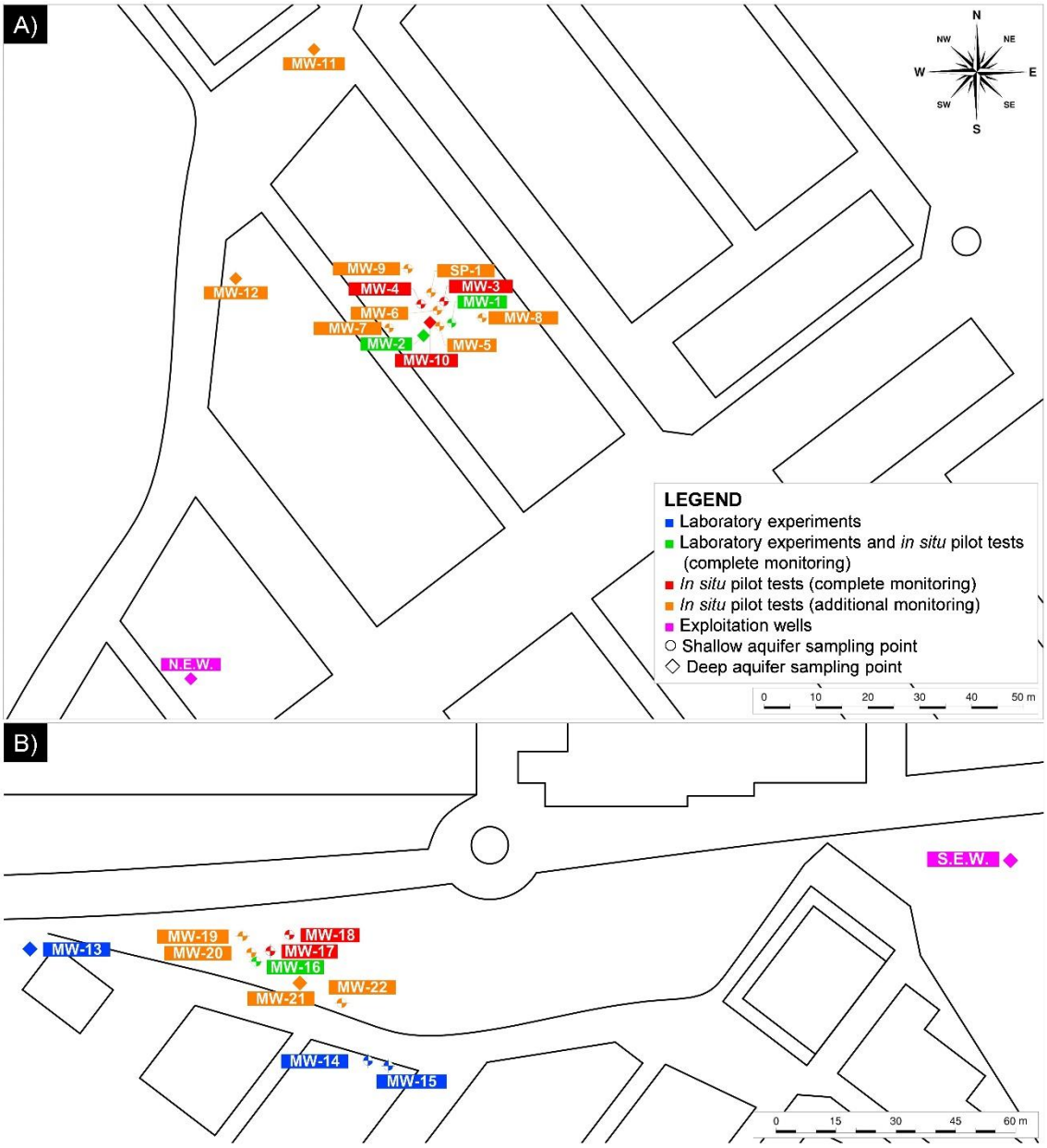


Fig. 1. Location of all the studied piezometers at the site: (A) north plume, (B) south plume. All sampling points used for groundwater collection for the laboratory microcosms and the monitoring of the in situ pilot tests are indicated. See figure legend for colour coding. See Table S1 for the constructive details of piezometers used in the in situ pilot tests.

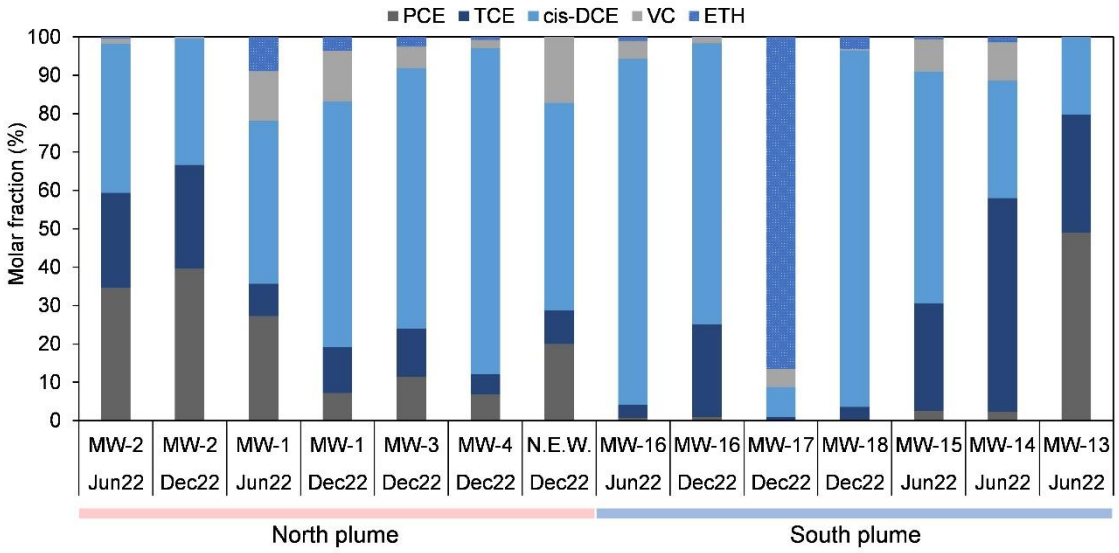


Fig. 2. Molar fraction (in %) of CEs and ETH in groundwater samples collected at the site in June and December of 2022, prior to the start of the in situ remediation pilot tests. See figure legend for colour coding.

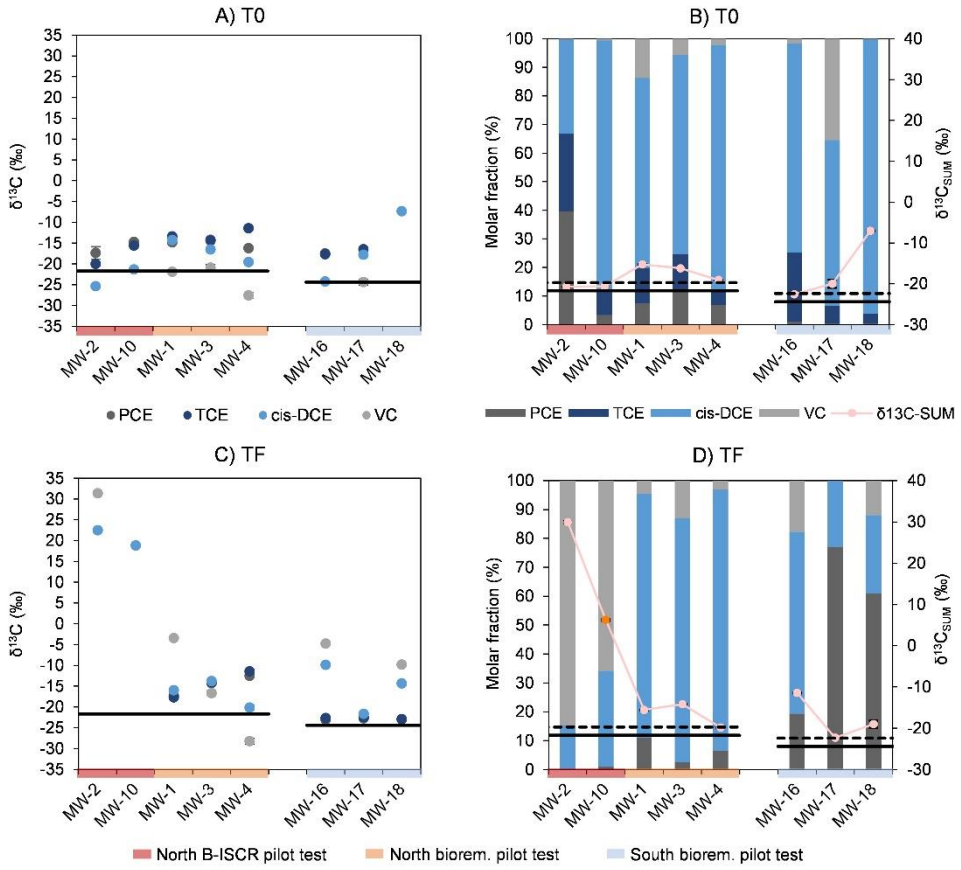


Fig. 3. Isotopic results in the studied piezometers prior (T0, December 2022) and after (TF) the in situ remediation pilot tests. $\delta^{13}C$ of CEs (A, C), and molar fraction of CEs and isotopic mass balance ($\delta^{13}C_{SUM}$) (B, D) are shown. See figure legend for colour coding. Error bars show the standard deviation of the replicate $\delta^{13}C$ analyses (A, C) and the error associated with the calculation of $\delta^{13}C_{SUM}$ (B, D). In most cases, error bar is smaller than the symbol. Solid black lines show $\delta^{13}C_{SUM}$ representative of the source zones (SI section 1.4) and dashed black lines show a deviation ($\Delta\delta^{13}C$) of +2‰ with respect to reference $\delta^{13}C_{SUM}$ values.

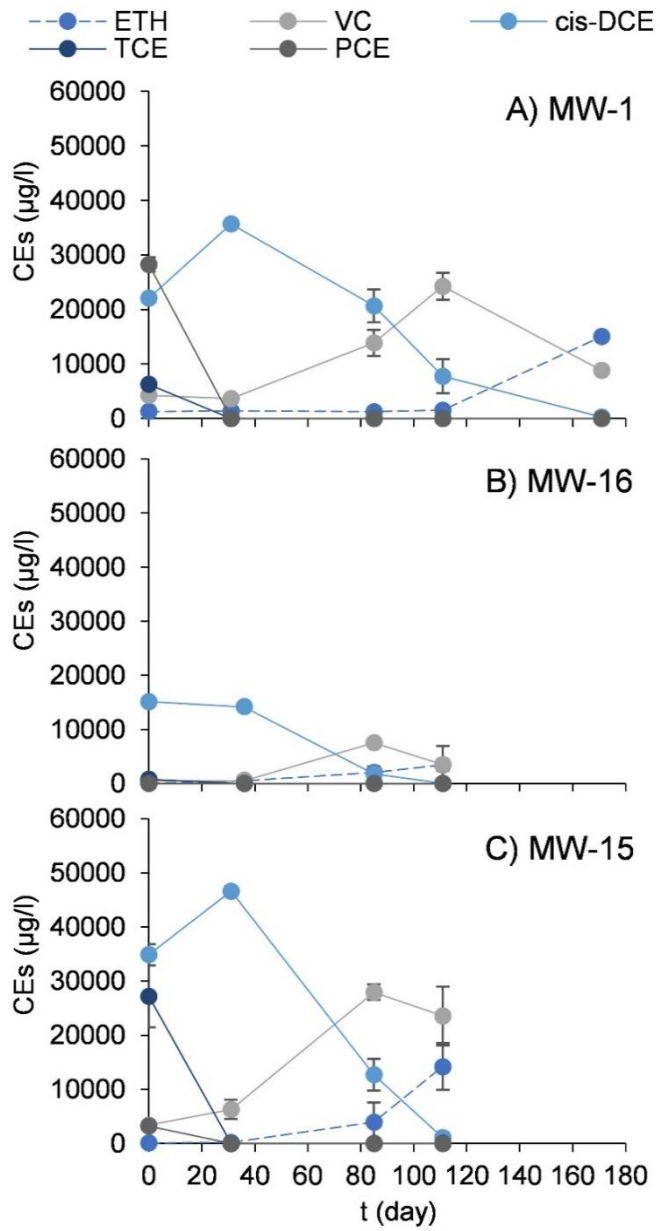


Fig. 4. Time-course of CEs and ETH concentration in lactate-amended microcosms prepared with groundwater from piezometers A) MW-1 (north shallow aquifer), B) MW-16 (south shallow aquifer), and C) MW-15 (south shallow aquifer). See figure legend for colour coding. Concentrations of CEs and ETH are presented as nominal concentrations. Data presented are the average of triplicate microcosms for MW-1 and MW-15, and duplicate for MW-16. Error bars show one standard deviation (1σ) for replicates. In some cases, error bars are smaller than the symbol itself.

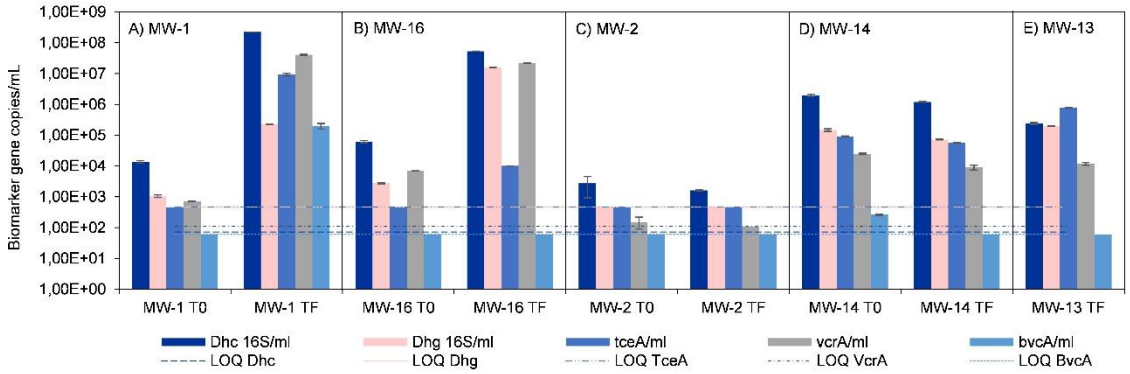


Fig. 5. Abundance of Dhg 16S rRNA and Dhc 16S rRNA gene copies, and the reductive dehalogenase genes tceA, vcrA and bvcA, from the lactate-amended microcosms that contained groundwater from piezometers A) MW-1 (north shallow aquifer), B) MW-16 (south shallow aquifer), C) MW-2 (north deep aquifer), D) MW-14 (south shallow aquifer), and E) MW-13 (south deep aquifer), in initial (T0) and final (TF, 150 days) samples. LOQ of assays are also indicated. See figure legend for colour coding. Data presented are the average of replicate measurements and include error bars showing the one standard deviation (1σ) for replicates.

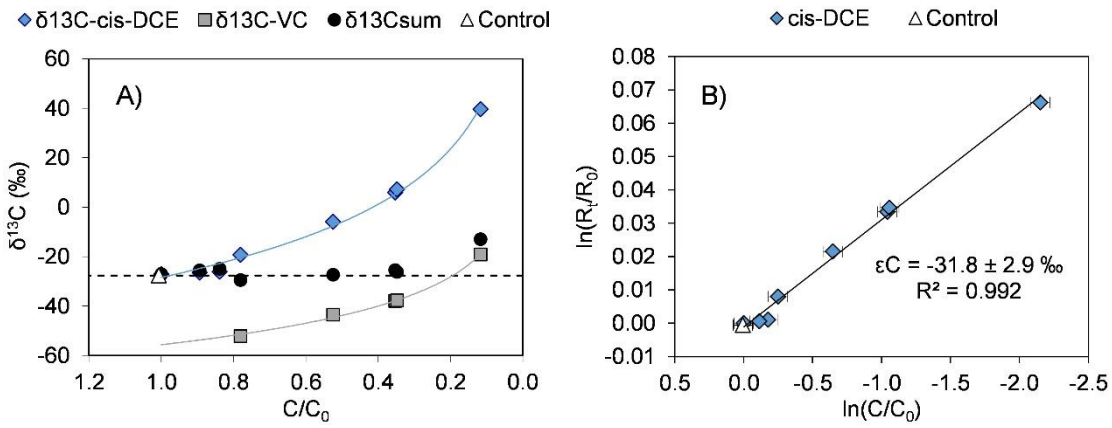


Fig. 6. Carbon isotope composition (A) and double logarithmic Rayleigh plot (B) for the anaerobic degradation of cis-DCE by the autochthonous CEs-degrading bacteria from piezometer MW-1. See figure legend for colour coding. Error bars stand for the standard deviation of duplicate measurements for $\delta^{13}C_{cis\text{-}DCE}$ *and* $\delta^{13}C_{VC}$*, and for the uncertainty calculated by error propagation for* $\delta^{13}C_{SUM}$ *and for the logarithmic plot.*

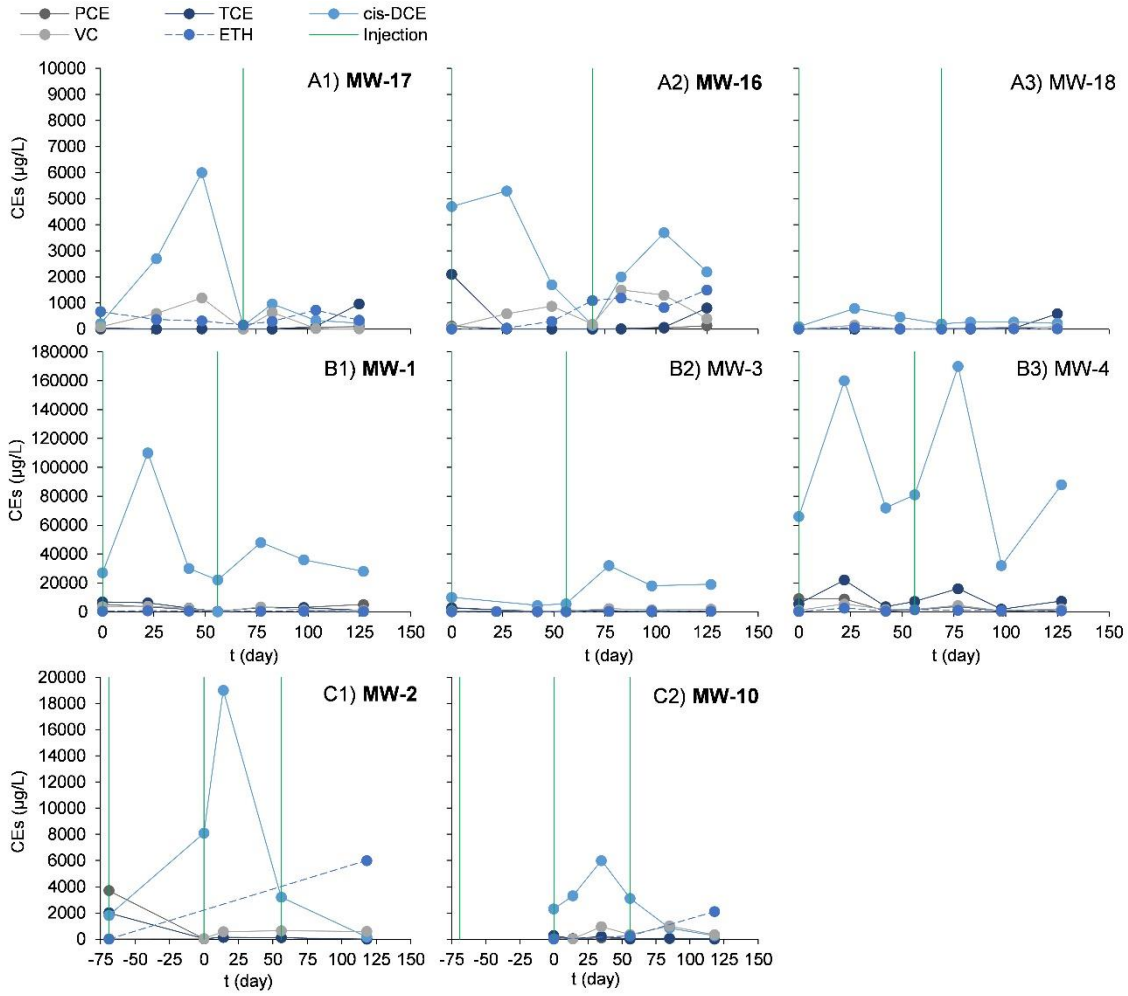


Fig. 7. Time-course of CEs and ETH at the monitoring wells during the three ERD pilot tests: (A) south shallow aquifer bioremediation; (B) north shallow aquifer bioremediation, and (C) north deep aquifer B-ISCR. See figure legend for colour coding. Injection wells are shown in bold. Two lactate injections (green vertical lines) were performed in the bioremediation pilot tests, whereas a first lactate injection (in MW-2) was followed by two combined lactate and sulfidized mZVI injections (in MW-10) in the B-ISCR pilot test. Data presented correspond to single measurements per each sampling campaign.

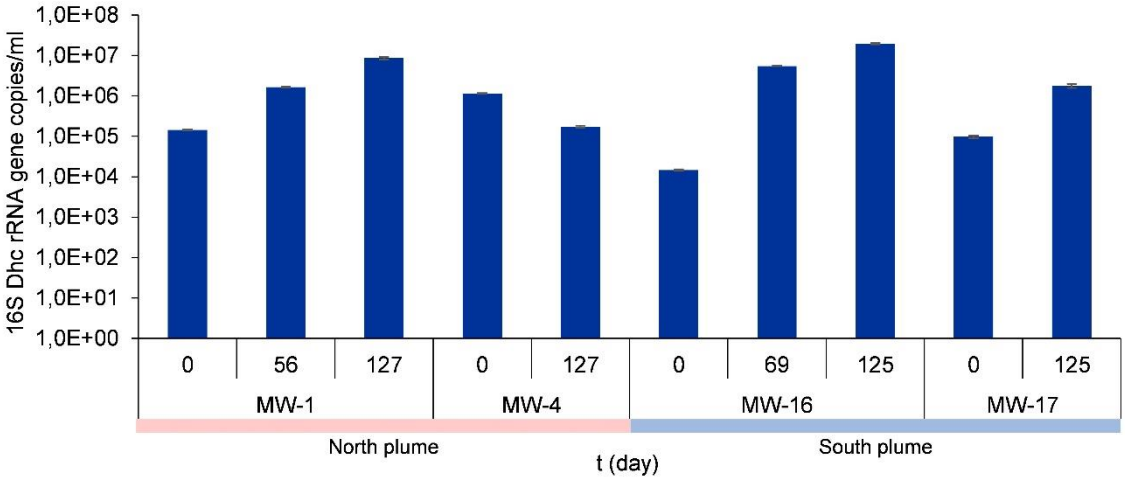


Fig. 8. Abundance of Dhc 16S rRNA gene copies in groundwater at different times (initial, middle and final sampling of the pilot tests, in days) at the north (MW-1 and MW-4) and south (MW-16 and MW-17) bioremediation pilot tests. Data presented is the average of replicate measurements and includes error bars showing the one standard deviation (1σ) for replicates.

Figure file with track changes Click here to access/download;Figure;renamed_8a973.docx

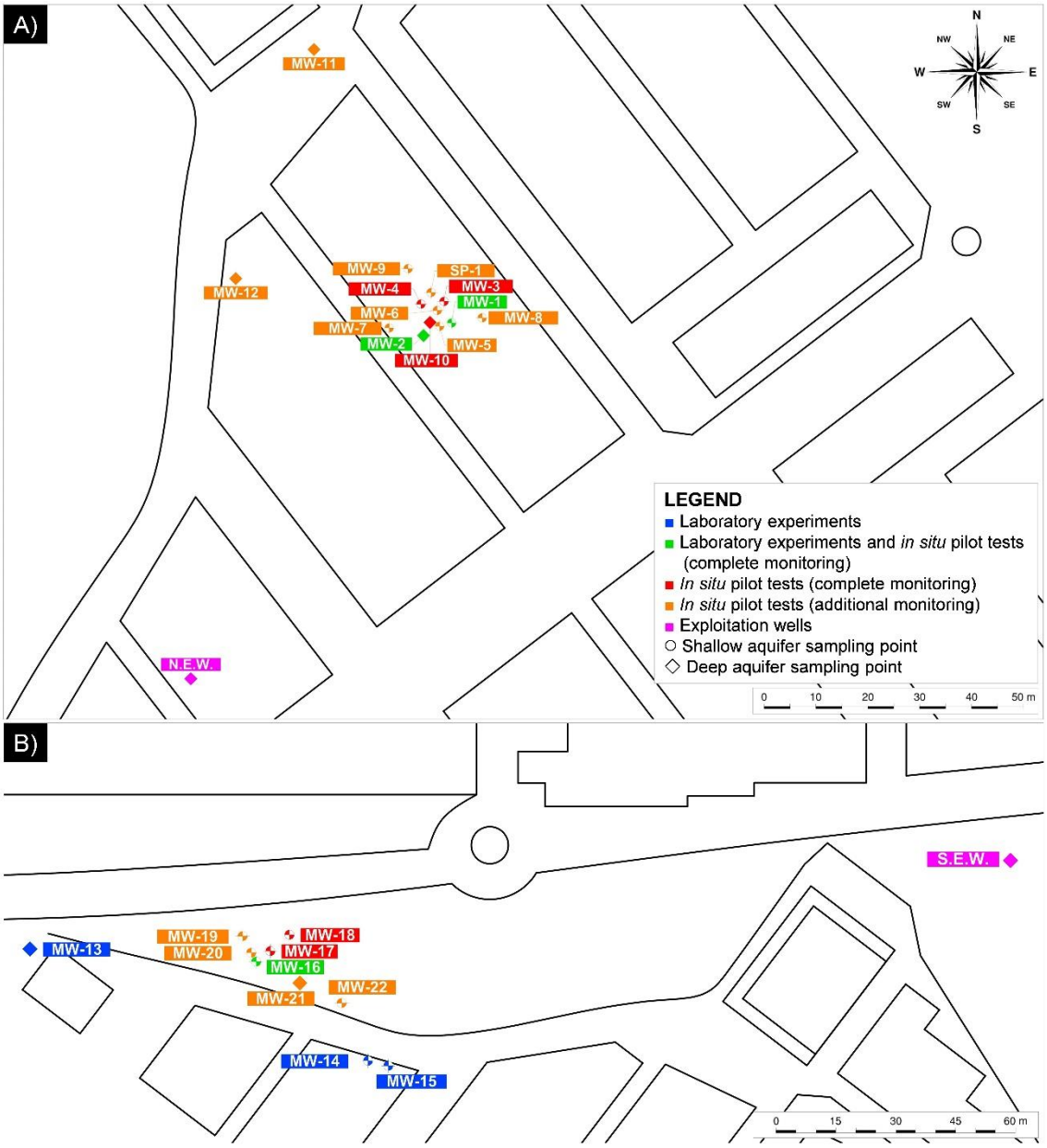


Fig. 1. Location of all the studied piezometers at the site: (A) north plume, (B) south plume. All sampling points used for groundwater collection for the laboratory microcosms and the monitoring of the in situ pilot tests are indicated. See figure legend for colour coding. See Table S1 for the constructive details of piezometers used in the in situ pilot tests.

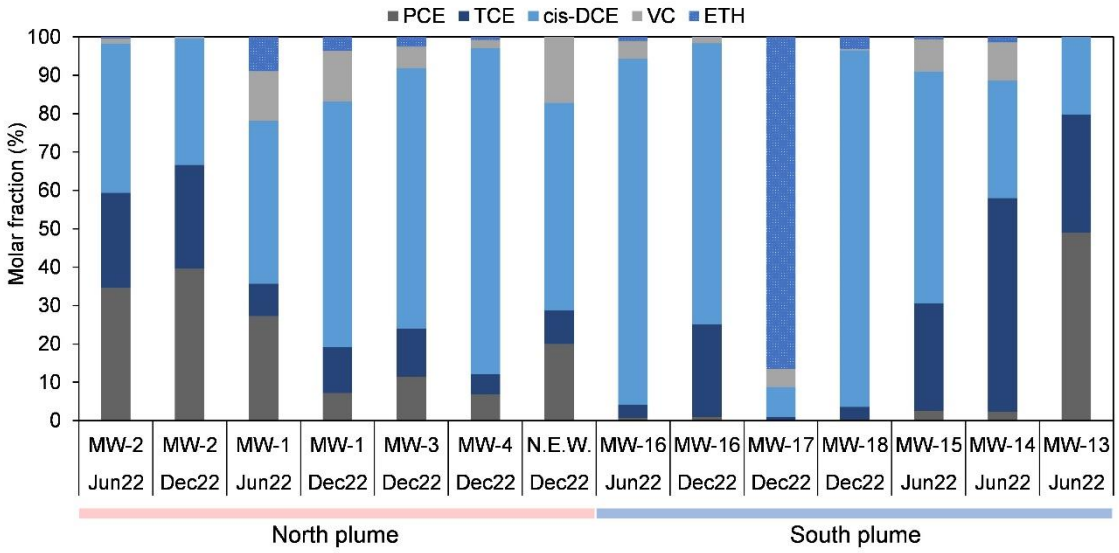


Fig. 2. Molar fraction (in %) of CEs and ETH in groundwater samples collected at the site in June and December of 2022, prior to the start of the in situ remediation pilot tests. See figure legend for colour coding.

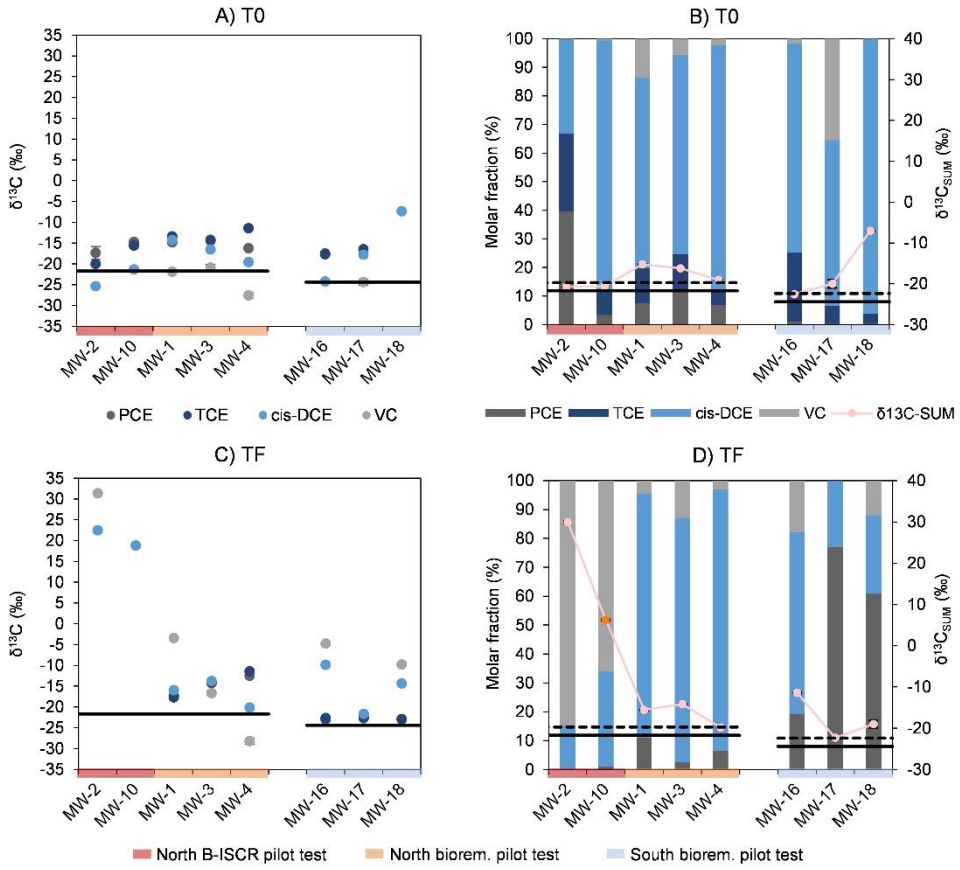

A) T0
B) T0
C) TF
D) TF
δ13C (‰)
Molar fraction (%)
δ13CSUM (‰)
MW-2
MW-10
MW-1
MW-3
MW-4
MW-16
MW-17
MW-18
PCE
TCE
cis-DCE
VC
δ13C-SUM
North B-ISCR pilot test
North biorem. pilot test
South biorem. pilot test

Fig. 3. ~~Panels A and B:~~ Isotopic results in the studied piezometers prior (T0, December 2022) and after (TF) the in situ remediation pilot tests. ~~(~~$\delta^{13}C$~~)~~ of CEs (A, C), and molar fraction of CEs and isotopic mass balance ($\delta^{13}C_{SUM}$) (B, D)~~,~~ are shown ~~in the studied piezometers prior (T0) the in situ remediation pilot tests (December 2022 campaign). Panels C and D: Isotopic results ($\delta^{13}C$) of CEs (C), and molar fraction of CEs and isotopic mass balance ($\delta^{13}C_{SUM}$) (D), in the studied piezometers after (TF) the pilot tests~~. See figure legend for colour coding. ~~For panels A and C, e~~Error bars show the standard deviation of the replicate $\delta^{13}C$ analyses (A, C)~~.~~ ~~In most cases, the error bar is smaller than the symbol itself. For panels B and D, error bars show~~and the error associated with the calculation of $\delta^{13}C_{SUM}$ (B, D)~~.~~ ~~estimated by error propagation, and assuming an error in concentration measurement of 10%.~~ In most cases, ~~the~~ error bar is smaller than the symbol. ~~The value of $\delta^{13}C_{SUM}$ for MW-10 (marked in salmon) presents greater uncertainty because the contribution of $\delta^{13}C_{VC}$ in $\delta^{13}C_{SUM}$, which could be significant given the molar fraction of VC, has not been considered (Table S7). For all panels: s~~Solid black lines show $\delta^{13}C_{SUM}$ representative of the ~~north ($\delta^{13}C_{SUM}$ = -21.7‰) and the south ($\delta^{13}C_{SUM}$ = -24.4‰)~~ source zones (SI section 1.~~3~~4) and~~.~~ ~~D~~dashed black lines ~~in panels B and D~~ show a deviation ($\Delta\delta^{13}C$) of +2‰ with respect to reference $\delta^{13}C_{SUM}$ values~~, the threshold for which the deviation is considered to be significant for environmental water samples, according to the EPA guide (Hunkeler et al., 2008)~~.

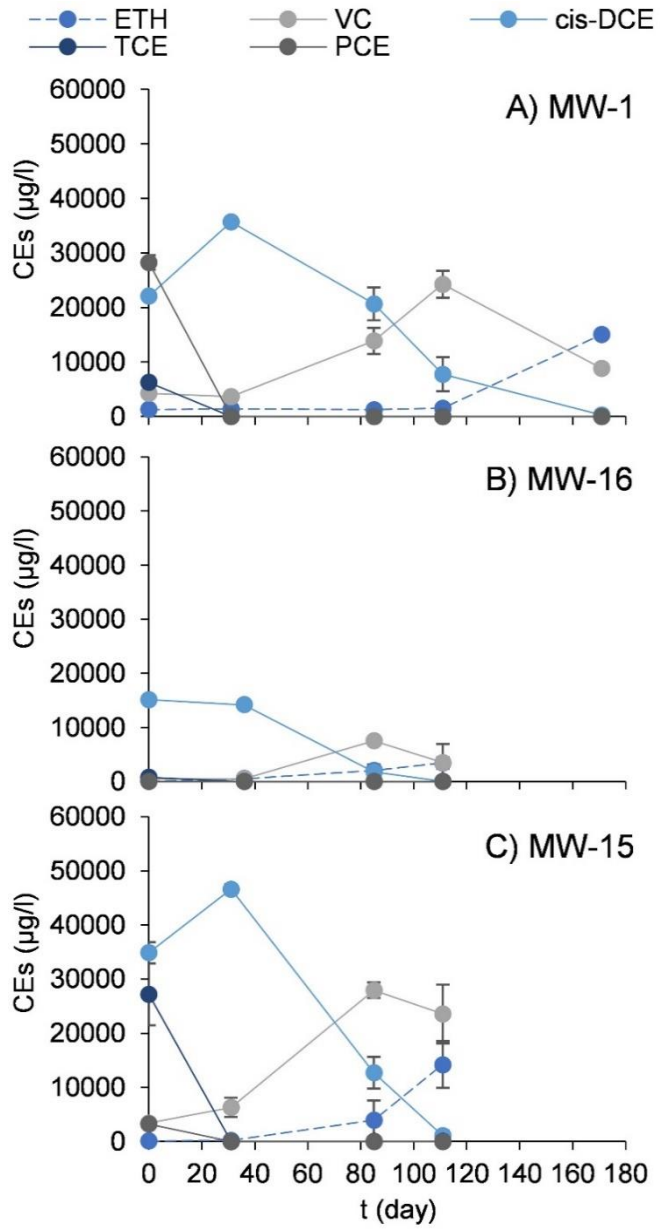


Fig. 4. Time-course of CEs and ETH concentration in lactate-amended microcosms prepared with groundwater from piezometers A) MW-1 (north shallow aquifer), B) MW-16 (south shallow aquifer), and C) MW-15 (south shallow aquifer). See figure legend for colour coding. Concentrations of CEs and ETH are presented as nominal concentrations. Data presented are the average of triplicate microcosms for MW-1 and MW-15, and duplicate for MW-16. Error bars show one standard deviation (1σ) for replicates. In some cases, error bars are smaller than the symbol itself.

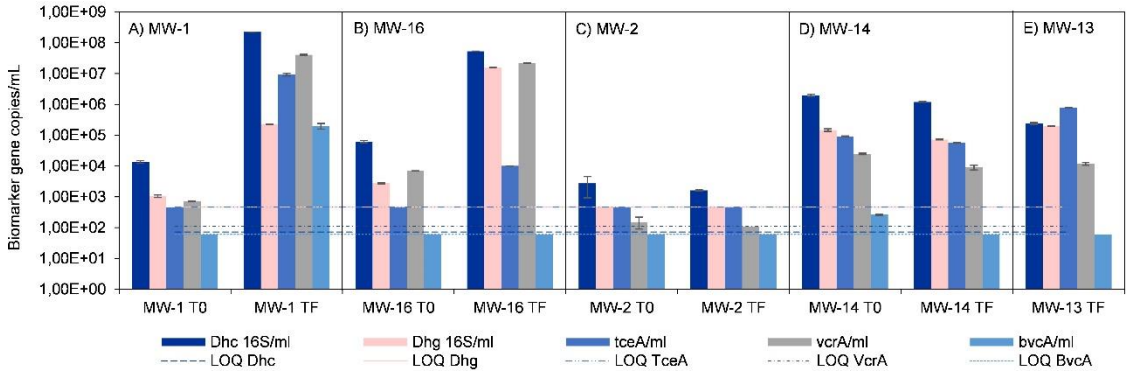


Fig. 5. Abundance of Dhg 16S rRNA and Dhc 16S rRNA gene copies, and the reductive dehalogenase genes tceA, vcrA and bvcA, from the lactate-amended microcosms that contained groundwater from piezometers A) MW-1 (north shallow aquifer), B) MW-16 (south shallow aquifer), C) MW-2 (north deep aquifer), D) MW-14 (south shallow aquifer), and E) MW-13 (south deep aquifer), in initial (T0) and final (TF, 150 days) samples. LOQ of assays are also indicated. See figure legend for colour coding. Data presented are the average of replicate measurements and include error bars showing the one standard deviation (1σ) for replicates.

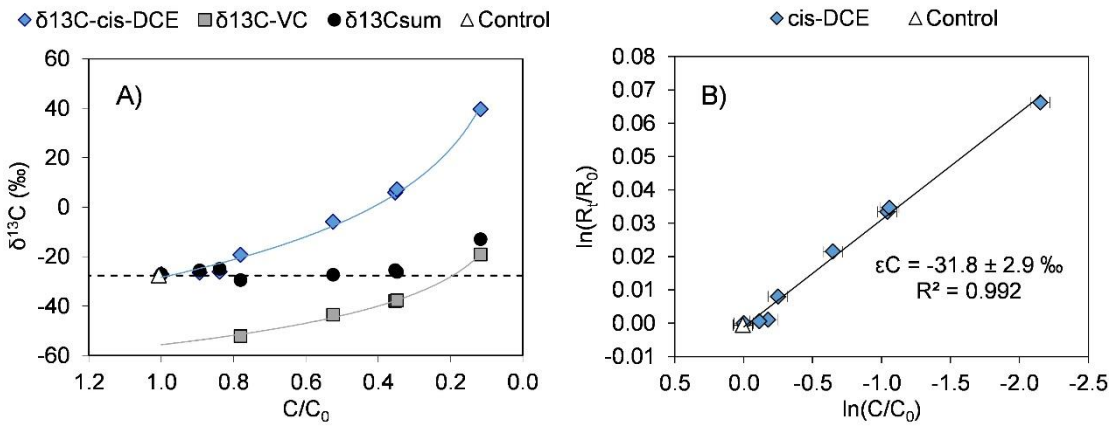


Fig. 6. Carbon isotope composition (A) and double logarithmic Rayleigh plot (B) for the anaerobic degradation of cis-DCE by the autochthonous CEs-degrading bacteria from piezometer MW-1. See figure legend for colour coding. Error bars stand for the standard deviation of duplicate measurements for $\delta^{13}C_{cis\text{-}DCE}$ *and* $\delta^{13}C_{VC}$*, and for the uncertainty calculated by error propagation for* $\delta^{13}C_{SUM}$ *and for the logarithmic plot.*

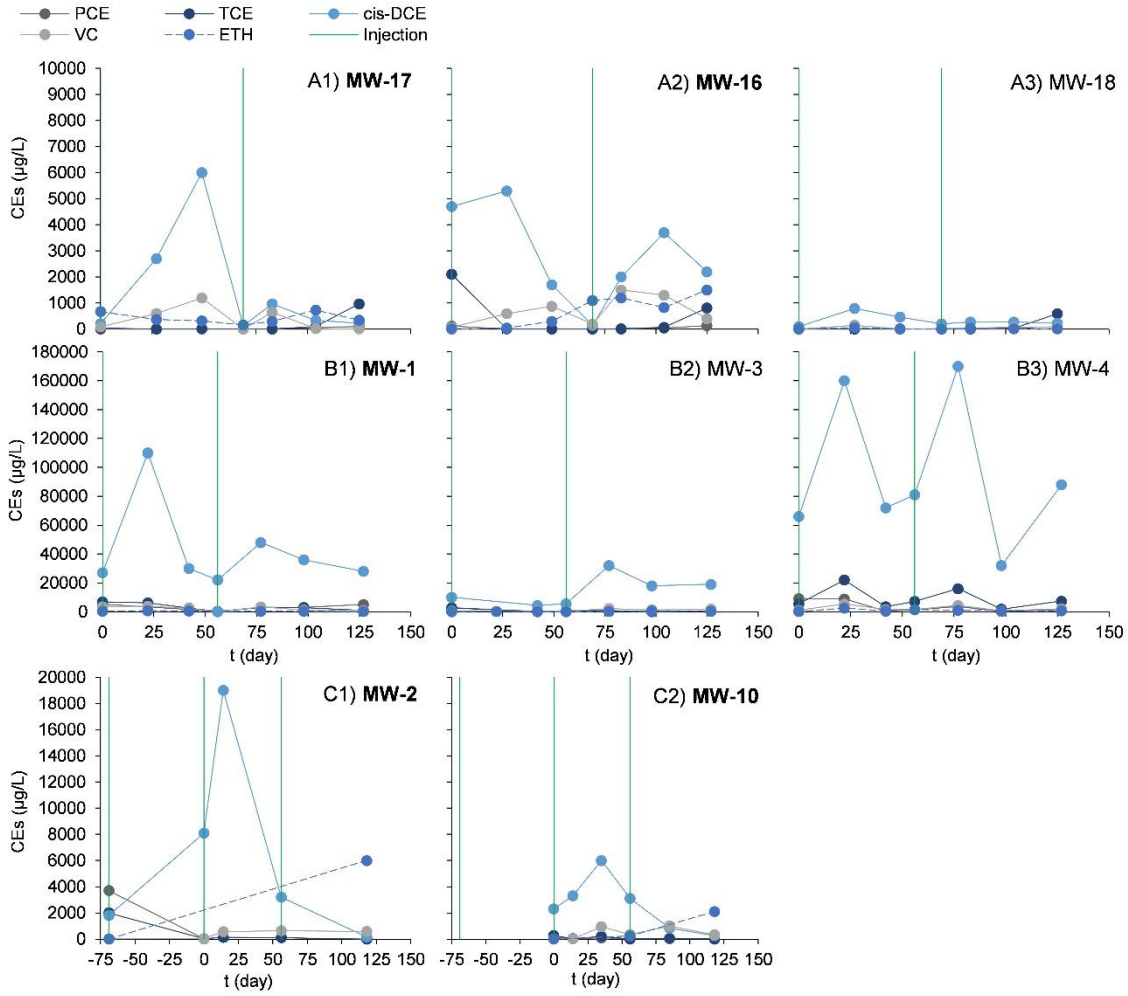


Fig. 7. Time-course of CEs and ETH at the monitoring wells during the three ERD pilot tests: (A) south shallow aquifer bioremediation; (B) north shallow aquifer bioremediation, and (C) north deep aquifer B-ISCR. See figure legend for colour coding. Injection wells are shown in bold. Two lactate injections (green vertical lines) were performed in the bioremediation pilot tests, whereas a first lactate injection (in MW-2) was followed by two combined lactate and sulfidized mZVI injections (in MW-10) in the B-ISCR pilot test. Data presented correspond to single measurements per each sampling campaign.

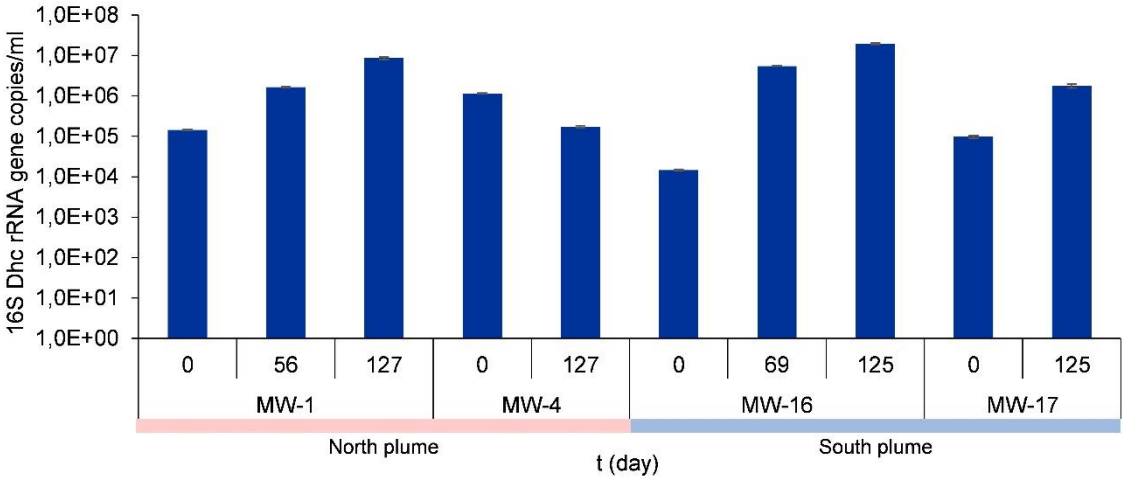


Fig. 8. Abundance of Dhc 16S rRNA gene copies in groundwater at different times (initial, middle and final sampling of the pilot tests, in days) at the north (MW-1 and MW-4) and south (MW-16 and MW-17) bioremediation pilot tests. Data presented is the average of replicate measurements and includes error bars showing the one standard deviation (1σ) for replicates.

Click here to access/download
Supplementary Material
renamed_56486.pdf

Declaration of interests

☒The authors declare that they have no known competing financial interests or personal relationships that could have appeared to influence the work reported in this paper.

☐The authors declare the following financial interests/personal relationships which may be considered as potential competing interests: